Department of Physics, Chemistry and Biology

Master's Thesis

# Search for Dark Matter in the Upgraded High Luminosity LHC at CERN

## Impact of ATLAS phase II performance on a mono-jet analysis

**Sven-Patrik Hallsjö**

Thesis work performed at Stockholm University

Linköping, June 4, 2014

LITH-IFM-A-EX--14/2863--SE



# Linköpings universitet
## TEKNISKA HÖGSKOLAN

Department of Physics, Chemistry and Biology

# Search for Dark Matter in the Upgraded High Luminosity LHC at CERN

## Impact of ATLAS phase II performance on a mono-jet analysis

**Sven-Patrik Hallsjö**

Thesis work performed at Stockholm University

Linköping, June 4, 2014

Supervisor: **Docent Christophe Clément**
FYSIKUM Stockholm University
**Professor Magnus Johansson**
IFM, Linköping University

Examiner: **Professor Magnus Johansson**
IFM, Linköping University

| | Avdelning, Institution<br>Division, Department<br><br>Theoretical physics group<br>Department of Physics, Chemistry and Biology<br>SE-581 83 Linköping | Datum<br>Date<br><br>2014-06-04 |
|---|---|---|

| | |
|---|---|
| **Titel**<br>Title | Sökandet efter mörk materia i den uppgraderade hög luminositets LHC i CERN<br>Search for Dark Matter in the Upgraded High Luminosity LHC at CERN |
| **Undertitel**<br>Subtitle | Påverkan av ATLAS fas II prestanda på en mono-jet analys<br>Impact of ATLAS phase II performance on a mono-jet analysis |
| **Författare**<br>Author | Sven-Patrik Hallsjö |

**Sammanfattning**
Abstract

The LHC at CERN is now undergoing an set of upgrades to increase the center of mass energy for the colliding particles to be able to explore new new physical processes. The focus of this thesis lies on the so called phase II upgrade which will preliminarily be completed in 2023. After this upgrade the LHC will be able to accelerate proton beams to such velocity that each proton has a center of mass energy of 14 TeV.

One disadvantage of this is that it will be harder for the ATLAS detector to isolate unique particle collisions since more and more collisions will occur simultaneously, so called pile-up.

For 14 TeV there does not exist a full simulation of the ATLAS detector. This thesis instead uses simulated data for the particle collisions and then uses so called smearing functions to emulate the detector responses.

This thesis focuses on how a mono-jet analysis looking for different WIMP models of dark matter will be affected by this increase in pile-up rate.

The models which are in focus are thoes which try to explain dark matter without adding new theories to the standard model or QFT, such as the effective theory D5 operator and light vector mediator models.

The limits set for the D5 operators mass suppression scale at 14 TeV and 1000 fb$^{-1}$ are 2-3 times better than previous results at 8 TeV and 10 fb$^{-1}$.

For the first time limits have been set on which mediator masses can be excluded for vector mediator models at 14 TeV.

**Nyckelord**
Keywords    ATLAS, Beyond standard model physics, CERN, Dark matter, Effective operator, Elementary particle physics, High energy physics, Mono-jet analysis, Vector mediator, WIMPS.

3

# Abstract

The LHC at CERN is now undergoing an set of upgrades to increase the center of mass energy for the colliding particles to be able to explore new new physical processes. The focus of this thesis lies on the so called phase II upgrade which will preliminarily be completed in 2023. After this upgrade the LHC will be able to accelerate proton beams to such velocity that each proton has a center of mass energy of 14 TeV.

One disadvantage of this is that it will be harder for the ATLAS detector to isolate unique particle collisions since more and more collisions will occur simultaneously, so called pile-up.

For 14 TeV there does not exist a full simulation of the ATLAS detector. This thesis instead uses simulated data for the particle collisions and then uses so called smearing functions to emulate the detector responses.

This thesis focuses on how a mono-jet analysis looking for different WIMP models of dark matter will be affected by this increase in pile-up rate.

The models which are in focus are thoes which try to explain dark matter without adding new theories to the standard model or QFT, such as the effective theory D5 operator and light vector mediator models.

The limits set for the D5 operators mass suppression scale at 14 TeV and 1000 $\text{fb}^{-1}$ are 2-3 times better than previous results at 8 TeV and 10 $\text{fb}^{-1}$.

For the first time limits have been set on which mediator masses can be excluded for vector mediator models at 14 TeV.

# Acknowledgments

v

# Contents

# Notation

**NOTATIONS**

| Notation | Explanation |
|---|---|
| barn(b) | 1 barn(b)$= 10^{-24}$ cm$^2$ |
| $\oplus$ | $a \oplus b = \sqrt{a^2 + b^2}$, $a \oplus b \oplus c = \sqrt{a^2 + b^2 + c^2}$ |

**ABBREVIATIONS**

| Abbreviation | Expansion |
|---|---|
| ATLAS | A large Toroidal LHC ApparatuS |
| CERN | Organisation européenne pour la recherche nucléaire[1] |
| CMS | Compact Muon Solenoid |
| CR | Control Region |
| LHC | Large Hadron Collider |
| MC | Monte Carlo |
| RMS | Root Mean Square |
| SM | the Standard Model of particle physics |
| SR | Signal Region |
| WIMP | Weakly Interacting Massive Particle |
| WIMPS | Weakly Interacting Massive ParticleS |
| QED | Quantum ElectroDynamics |
| QFT | Quantum Field Theory |
| QM | Quantum Mechanics |

---

[1]Originally, Conseil Européen pour la Recherche Nucléaire

# 1

# Introduction

Discrepancies in measurements of the rotations of galaxies indicate the presence of a large amount of matter which interacts through gravity, though not electromagnetically making it invisible to our telescopes. This matter is commonly referred to as dark matter. Since no known or hypothesized particle in the standard model of particle physics can be used as a candidate for dark matter, this hints at the presence of new physics.

At the Organisation Européene pour la Recherche Nucléaire (CERN) focus lies among other things to discover any evidence of so called weakly interacting massive particles (WIMPS) which may be a candidate for dark matter. It is impossible to electromagnetically detect any interaction of dark matter candidates on the subatomic scale. However through using existing theoretical frameworks as templates to design searches by searching for assumed decay channels and by investigating what is invisible to the ATLAS and CMS detectors. By using momentum conservation it is hoped that signs will be found. Though to date no candidates for WIMPS have been found nor any other explanation of dark matter.

Current experiments at CERN and current theories now show that higher energies are required at the LHC to be able to see any signs of WIMPS. This is why the LHC and all detectors are undergoing a vast upgrade program [1]. In this thesis focus will be on the last part of the upgrade due for completion in 2023, known as the high luminosity-LHC phase II upgrade; and also on the ATLAS detector. The method used in this thesis focuses on looking at data which emulate conditions at the upgraded LHC.

## 1.1   Research goals

This research took place at Stockholm University from January 7th until May 16th. During the research period the following tasks were set up and performed or answered:

- Implement a C++ programme that loops over the collisions inside the signal and background datasets.

- For each collision retrieve the relevant observables (variables used to extract the signal over the background) and apply "smearing functions" to emulate the effect of the high luminosity on the observables.

- For both signal and background datasets, compare observables before and after smearing. What observables are the least/most affected?

- Implement selection criteria that selects the signal collisions efficiently while reduces significantly the background. In a first step the selection criteria should be taken from existing studies.

- Selection criteria can be evaluated and compared with each other using a figure of merit p, that measures the sensitivity of the experiment to the dark matter signal. Calculate p for the given selection criteria before and after smearing.

- What is the effect of the high luminosity (smearing) on the value of p?

- Investigate other selection criteria and observables, to mitigate the effect of high luminosity. Use p to rank different criteria after smearing.

- Conclude on the effect of the high luminosity on the sensitivity for dark matter and possible ways to mitigate its effects using alternative observables and selection criteria.

## 1.2  Theoretical Background

### 1.2.1  Quantum mechanics and quantum field theory

In the beginning of the 20th century, some physical phenomena could not be explained by classical physics, for example the ultra-violet disaster of any classical model of black-body radiation, and the photoelectric effect [2]. It was these phenomena that led to the formulation of quantum mechanics (QM), where energy transfer is quantized and particles can act as both waves and particles at the same time [3].

Combining QM with classical electromagnetism proved harder than expected, colliding a photon(em-field) and an electron (particle/wave) is quite tricky. This can be seen when trying to calculate the scattering between them both in a QM schema. One idea that came from this was to explain them both in the same framework, field theory. Also, trying to incorporate special relativity into QM suggested a field description where space-time is described using the metric formalism from differential geometry. The culmination of both of these problems is the first part of a Quantum field theory (QFT), Quantum electrodynamics (QED) which with incredible precision explains electromagnetic phenomena including effects from special relativity [4]. It is in this merging that antimatter was theorised, since it is a requirement for the theory to hold. After the discovery of antimatter, QED was assumed to give a correct description of the phenomena around us. Since then the theory has been altered somewhat to explain more and more experimental data. This is discussed more in subsection 1.2.2 and subsection 1.2.3.

To be able to calculate properties in QFT one uses the Lagrangian formalism [5], which gives a governing equation for the different physical processes. In general the Lagrangian used for the Standard model is quite complicated, one can thus focus on one of the different terms corresponding to a specific interaction. This can be done to calculate the so called cross-section for a process.
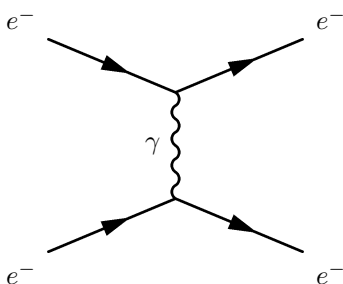


**Figure 1.1:** *An example of a Feynman diagram explaining an electron-electron scattering using QED.*

For a particle collision [6], the cross-section can be seen as a measure of the effective surface area seen by the impinging particles and as such is expressed in units of area. The cross section is proportional to the probability that an interaction will occur. It also provides a measure of the strength of the interaction between the scattered particle and the scattering center. A step to simplify the

calculation of the cross-sections is to use so called Feynman diagrams, an example of which is given in figure 1.1. Through the figure, which comes with certain rules, and knowing what the major process (in this case QED) one can calculate the cross-section [4, 6]. It is this which is needed to predict the detection of new particles.

### 1.2.2   Nuclear, particle and subatomic particle physics

Many could argue that these branches of physics started after Ernest Rutherford famous gold foil experiment [7], where he discovered that matter is composed of matter with a nucleus, a lot of empty space and electrons.

It was this that sparked the curiosity to see what the nucleus is made of and what forces govern the insides of atoms. After this, and the combination of the theoretical description given by QM, a lot more has been discovered and still more has been predicted. The newest of these is of course the Higgs particle, which was predicted through QFT and then discovered by the ATLAS and the CMS experiments at CERN [8, 9].

It is know known that all discovered particles are built up of fundamental particles, it is that that builds up the standard model [7].

### 1.2.3   The standard model of particle physics

To date there are two fundamental types of particles which are modelled as point like, quarks and leptons, seen in figure 1.2. Aside from this and also seen in the figure are the gauge bosons which are carriers of the different forces.

All other known particles are built up by these fundamental particles. These combined particles are often divided into different groups depending on the fundamental particles that build them up. For instance, particles build up of three quarks are known as hadrons. Particles with an integer spin are known as bosons whereas half-integer particles are known as fermions.

The standard model of particle physics, referred to simply as the standard model (SM), is a model which tries to categorize all the fundamental particles that have been discovered experimentally. QFT explains the interactions between these particles and it has also predicted several particles by including symmetries [7].

SM is today the pinnacle of particle physics and can be used to explain almost everything that occurs around us. There are however some problems [11]:

- There is no link between gravity and the SM.

- Asymmetry between matter and antimatter can not be fully explained.

- No explanation that can contain dark matter.

In this thesis focus lies with dark matter, some more introduction to possible dark matter and different candidates in extensions to SM are explained in subsection 1.2.4.
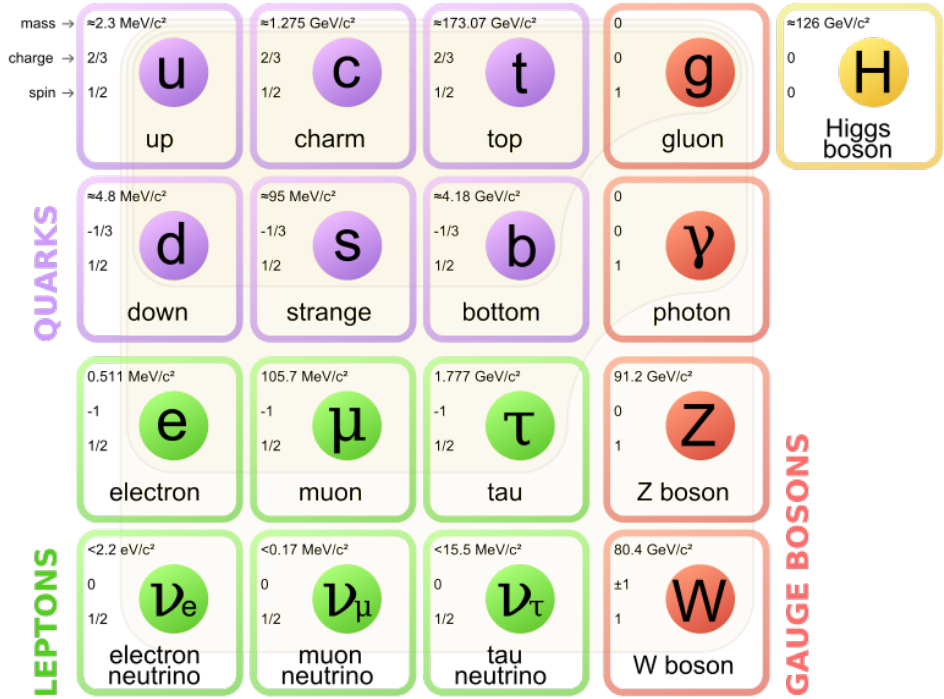
**Figure 1.2:** *The standard model of particle physics where the three first columns represent the so called generations, starting with the first [10].*

## 1.2.4   Dark matter

Dark matter is the name given to, among other things, the solution to the discrepancies of galactic rotations [12].

The presence of dark matter can be measured indirectly from its gravitational effects. Focus on matter in a galaxy which are rotating around the center of the galaxy. Through Newtons law of gravity and the centrifugal force one can calculate the rotation speed as a function of the distance to the center of the galaxy. Since one of these forces is attractive and the other repulsive, if the matter is in a stable orbit around the galactic center they must be equal and give us an expression for the speed depending on the distance. Newtons law can be written as the following:

$$F_{Gravitational} = G\frac{Mm}{r^2} \equiv G_M\frac{m}{r^2} \qquad F_{Centrifugal} = m\frac{V^2}{r} \qquad (1.1)$$

where $G$ is the gravitational constant, $M$ the mass of the centre object, $m$ the mass of the matter, $r$ the distance between the two and $V$ is the rotation speed. It has been simplified using $G_M$ since all matter orbits the same galactic center. Setting

the equations in (1.1) results in:

$$G_M \frac{m}{r^2} = m\frac{V^2}{r} \Leftrightarrow V^2 = \frac{G_M}{r} \Rightarrow V = \sqrt{\frac{G_M}{r}} \propto \frac{1}{\sqrt{r}} \tag{1.2}$$

where the speed is assumed to be positive and $\propto$ means proportional. Through these simple calculations it is shown that the rotation speed should decrease with and increased distance. The same reasoning can be applied to our solar system where this is the case figure 1.3a. The relation in these units is $V = \frac{107}{\sqrt{r}}$ where 107 can be used in (1.2) to calculate the mass of the sun. However when looking at galaxies, even when taking into account that one has to see the galaxies as a mass distribution and that the above is only true when outside of the inner mass half, this is not the case! In figure 1.3b experimental data can be seen from the galaxy NGC3198 with a fitted curve which does not decrease with the distance but is instead constant. This is the discrepancy which is solved by postulating the existence of dark matter [13]. After this the big question arises, what could this
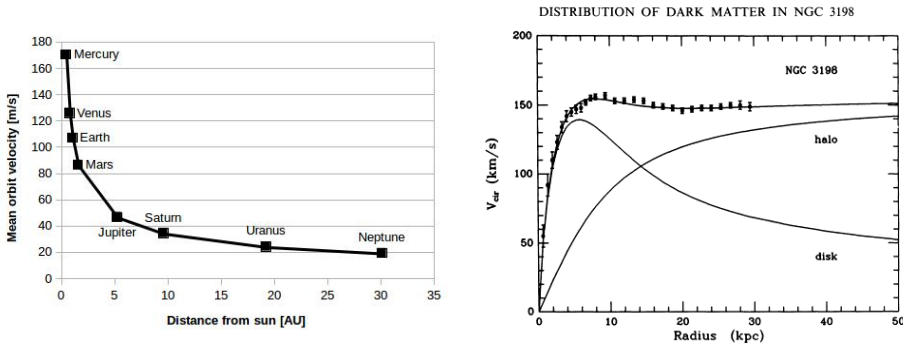


**(a)** *Rotation speed of planets in our solarsystem. Since the distance is quite small on an astronomical scale, there is no sign of dark matter. Based on data from [14].*

**(b)** *Rotation speed of mater in NGC3198 with a curve fitting and three different models, if only a dark model halo existed, if there was no dark matter and the correct, if both exist [15].*

**Figure 1.3:** *Different rotation curves, both for planets in our solar system and matter in the NGC3198 galaxy.*

dark matter consist of? What is known so far lies in the name. It is called dark since there is no electromagnetic interaction and matter since it has gravitational interaction. This means that it can not be made up of anything in the Standard Model apart from neutrinos. Astrophysical measurements have also indicated that dark matter can not be fully explained as being neutrinos nor baryonic matter [16]. This means that dark matter can not be made out of any standard model particles.

The main interest of this thesis and also the main contributor to the rotational discrepancies is known as cold dark matter. This is due to the matter having a

279 low speed, thus low kinetic energy, and have a high particle mass (In the GeV
280 scale) [11, 17, 18]. There are several strategies to search for dark matter, [11]

281 • Ordinary matter interacting with ordinary matter can produce dark matter,
282   known as production. This is the processes that occurs at particle accelera-
283   tors is the method explored in this thesis.

284 • Dark matter interacting with ordinary matter can produce dark matter,
285   known as direct detection.

286 • Dark matter interacting with dark matter can produce ordinary matter,
287   known as indirect detection.

288 In this thesis the focus lies with production at colliders, namely the LHC. There
289 are several theories models for how to detect dark matter in proton-proton colli-
290 sions such that occur at the LHC at CERN. This is covered more in subsection 1.2.7.

## 1.2.5 Effective field theory

292 In quantum field theory the objective is usually to find the part of the Lagrangian
293 which explains a type of interaction, known as the operator of the interaction and
294 also to find the probability amplitude (cross-section) for a certain interaction.
295 For complicated processes it is easier to employ a simplified phenomenological
296 model. This is done by using an effective field theory and the concept is explained
297 in figure 1.4. The operator can be found through assuming the possible interac-
298 tions and using the effective field theory [4].



*(a) Electromagnetic interaction.*    *(b) Effective diagram of figure 1.4a.*
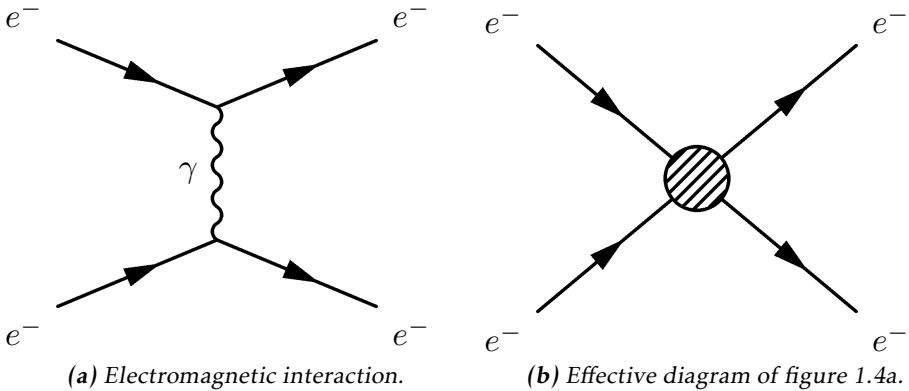
**Figure 1.4:** *Feyman diagram of an electron-electron scattering, both as a diagram where a photon is exchanged and as its effective theory version, where the details are hidden in the blob.*

299 In this thesis the same effective field theory as in Refs. [17, 19] is considered. The
300 WIMP (denoted $\chi$) is assumed to be the only particle in addition to the standard
301 model fields. In order to explain dark matter the WIMP $\chi$ must be stable. For this

reason only Feynman diagrams with an even number of $\chi$ are considered. It is assumed that the mediator exists is heavier that the WIMPS, meaning that their interactions are in higher order terms of the effective field theory and thus not included in the operators.

The operator used in this thesis are assumed to be quark bilinear operators on the form $\bar{q}\Gamma q$ where $\Gamma$ is a $4 \times 4$ matrix of the complete set,

$$\Gamma = \left\{1, \gamma^5, \gamma^\mu, \gamma^\mu \gamma^5, \sigma^{\mu\nu}\right\} \tag{1.3}$$

This will dictate how the operator is written, more of why this is done can be found in [4, 17, 19].

This defines an effective field theory of the interaction of singlet WIMPS with hadronic matter. It is an approximation which will break down when the mediator mass is close to the mass of the WIMP. The condition for this is derived in [19] and gives:

$$M > 2m_\chi \tag{1.4}$$

where $m_\chi$ is the mass of the WIMP and M is the mass of the mediator particle. There is also the requirement that:

$$M \lesssim 4\pi M_* \tag{1.5}$$

where $M_*$ is the energy scale where the effective theory is no longer a good approximation.

In this work, WIMPS are assumed to be Dirac fermions (half integer spin and is not its own antiparticle).

In table 1.1 the operator which is integrated out via the effective field theory and is of interest in this thesis are given.

| Name | Initial state | Type | Operator |
|------|---------------|------|----------|
| D5 | qq | vector | $\frac{1}{M_*^2}\bar{\chi}\gamma^\mu\chi\bar{q}\gamma_\mu q$ |

***Table 1.1:*** *Table based on discussion in [18].*

Where D denotes that the WIMPS are assumed to be Dirac fermions. These can all be described using figure 1.5a.
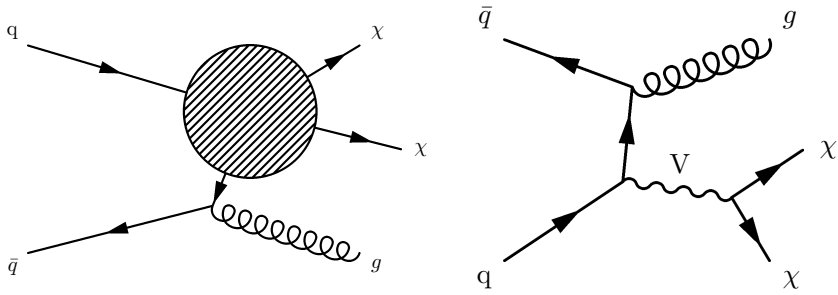
**(a)** *Effective Feynman diagram explaining the D-operators.*

**(b)** *Feynman diagram describing the vector mediator model.*

**Figure 1.5:** *Feynman diagrams describing the signal models used in this thesis.*

Another model which is considered is a vector mediator model which is described by figure 1.5b.

### 1.2.6   Jets

In particle collisions free gluons and quarks with high energy can be produced. According to QFT these can not exist and must decay through a process known as hadronization meaning that they will decay into a cone of energetic hadrons, which is known as a Jet. It is not possible to measure these free gluons or quarks, however this cone of hadrons will travel in the same direction and will be measured by the calorimeters, see subsection 1.3.2. These measurements can then be summed to calculate the energy and momentum which the initial gluon or quark had which in turn results in more information about the collision.

### 1.2.7   Search for WIMPS

The main problem with searching for WIMPS is that one is looking for a small signal among a lot of uninteresting proton-proton collisions. One way to search for WIMPS and overcome this difficulty is a so called mono-jet analysis which is described in subsection 1.3.5.

This method is a way to detect WIMP production among other proton-proton collision events and relies on the observation of high energetic jet, which arises from the gluon in both figures in figure 1.5, on one side and seemingly non conservation of energy or momentum, which will be denoted missing energy. This means that something has happened which the detectors can not detect. If the models from subsection 1.2.5 can explain the missing energy, then evidence for WIMP production would have been found.

Since the search for WIMPS at the LHC is based on looking at the missing energy, not actual detection, the experiment can not establish if a WIMP is stable on a

349 cosmological time scale and thus if it is a dark matter candidate [18]. This means
350 that if a candidate is found, it may still not be the dark matter that is needed to
351 explain the cosmological observations.

352 ATLAS has looked looked at proton-proton collisions, with 8 TeV center of mass
353 energy, which contain high energetic jets without finding any excess of mono-jet
354 events. This is why it is very interesting that the LHC is undergoing a upgrade
355 that will allow higher energy levels, see subsection 1.3.6. With this the processes
356 can be given higher energy and thus the produced particles can be comprised of
357 higher mass.

## **1.3   Experimental overview**

### **1.3.1   LHC**

The large hadron collider (LHC) is a particle accelerator located at CERN near
Geneva in Switzerland, see figure 1.6. The accelerator was built to explore physics
beyond the standard model and to make more accurate measurements of stan-
dard model physics. Before it was shut down for an upgrade in 2012 it was able
to accelerate two proton beams to such a velocity that each proton in them had
an energy of 4 TeV which gives a center of mass energy of $\sqrt{s} = 8$ TeV. The proton
beam is comprised of bunches of protons with enough spacing that bunch colli-
sions can happen independent of each other. The rate at which the accelerator
produces a certain process can be calculated through the instantaneous luminos-
ity. For the LHC the instantaneous luminosity was $10^{34}$ cm$^{-2}$s$^{-1}$ [20] or 10nb$^{-1}$s$^{-1}$
where 1 barn(b)= $10^{-24}$ cm$^2$.
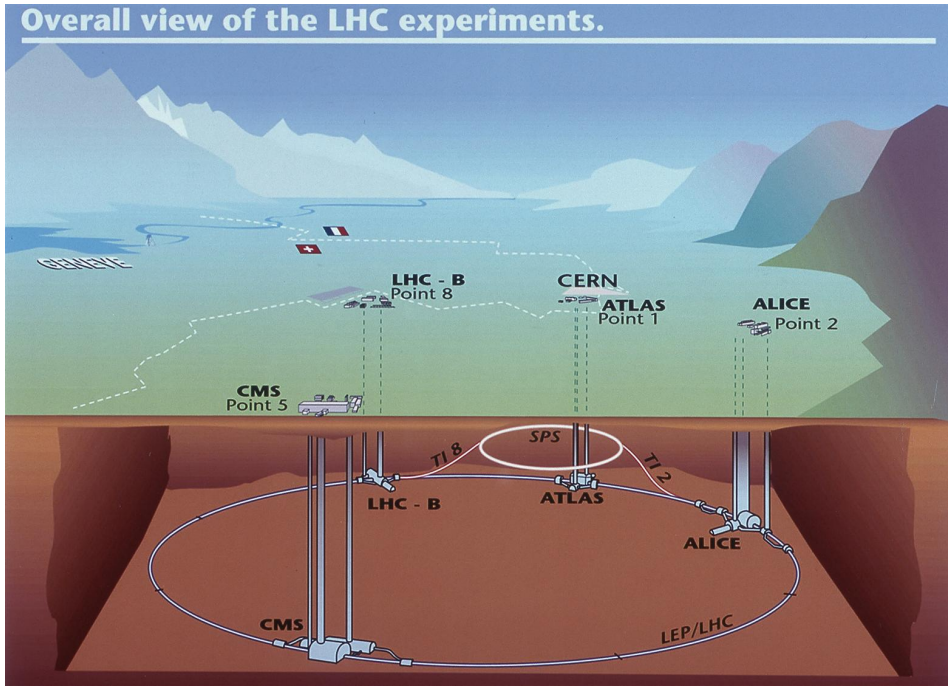


*Figure 1.6: Figure showing the LHC and the different detector sites[21].*

The instantaneous luminosity, often just denoted luminosity, can be defined in
different ways depending on how the collision takes place. For two collinear
intersecting particle beams it is defined as:

$$\mathcal{L} = \frac{f k N_1 N_2}{4\pi \sigma_x \sigma_y} \tag{1.6}$$

where $N_i$ are the number of protons in each of the bunches, f is the frequency at which the bunches collide , k the number of colliding bunches in each beam, and $\sigma_x$ ($\sigma_y$) is the horizontal (vertical) beam size at the interaction point. Since the instantaneous luminosity increases quadratically with more protons in each bunch, increasing the number of protons would be a good strategy to increase the instantaneous luminosity. However aside from the difficulties to create and maintain a beam with more particles, a large $N_i$ increases the probability for multiple collisions per bunch crossing, referred to as pile-up. Pile up will be a key aspect which is described more in subsection 1.3.4.

The expected number of events for a given physics process can be calculated by using the instantaneous luminosity, (1.6), through the following:

$$N = \sigma \int \mathscr{L} dt \equiv \sigma \mathcal{L} \tag{1.7}$$

where $\mathcal{L}$ is the integrated luminosity and $\sigma$ is the cross section which is often measured in barn. The integrated luminosity is a measurement of total number of proton-proton interactions that have occurred over time and is also a common measure of how much data was recorded. Before the LHC was shut down $\mathcal{L}$ was 20.8 fb$^{-1}$.

### 1.3.2 ATLAS

As seen in figure 1.6, there are several detectors at the LHC. One of these is ATLAS which is a general purpose detector that uses a toroid magnet. Its goal is to observe several different production and decay channels. The detector is composed of three concentric sub-detectors, the Inner detector, the Calorimeters and the Muon spectrometer [22].

The Inner detectors main task is to measure the tracks of the particles and measures position of the initial proton-proton collision. Aside from this it measures the track momenta and the charge of charged particles. It can however only detect charged particles.

The Calorimeters, electromagnetic and hadronic, are used to measure the energy contained in the different particles. The electromagnetic calorimeter is used to measure energy and direction of photons and electrons whereas the hadronic calorimeter is designed to measure the energy and direction of hadrons.

The Muon spectrometer is used to measure signs of muons, which will simply pass through the other detectors without leaving a trace. It also measures the energy and momentum of the muons.

The neutrinos escape the ATLAS experiment without being detected, and in this thesis it is assumed that WIMPS pass through all the detectors without leaving any trace.

Therefore WIMPS and neutrinos have the same detector signature. As seen in section 3.4 the main background to the WIMP signal is the production of a Z boson that in turn decay to two neutrinos mimicking the WIMP signature.

### 1.3.3   Coordinate system

The coordinate system of ATLAS, seen in figure 1.7 is a right-handed coordinate system with the x-axis pointing towards the centre of the LHC ring, and the z-axis along the tunnel/beam (counter clockwise) seen from above. The y-axis points upward. The origin is defined as the geometric center of the detector. A cylindrical coordinate system is also used for the transversal plane, (R,$\phi$,Z). For simplicity the pseudorapidity of particles from the primary vertex is defined as:

$$\eta = -\ln(\tan\frac{\theta}{2}) \tag{1.8}$$

where $\theta$ is the polar angle (xz-plane) of the particle direction measured from the positive z-axis. The difference in $\eta$ of two particles is through this definition invariant under Lorentz boosts in the z-direction.

It is quite common to calculate the distance between particles and jets in the $(\eta, \phi)$ space, $d = \sqrt{(\Delta\eta)^2 + (\Delta\phi)^2}$.
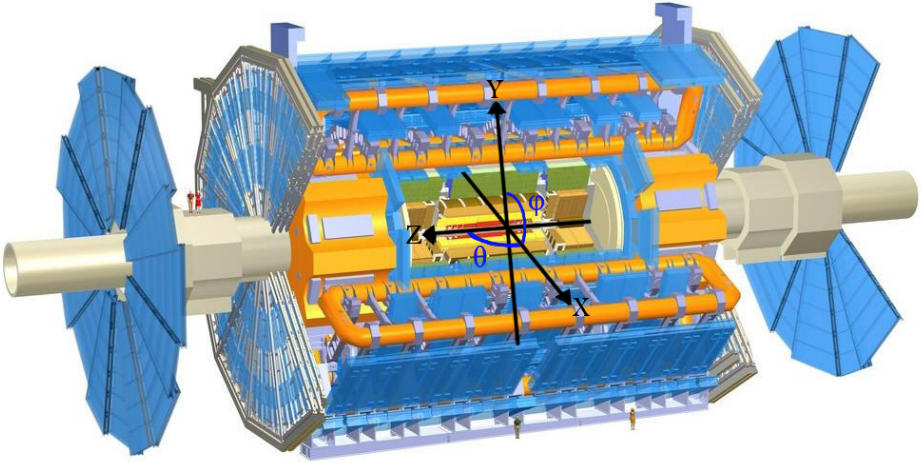


*Figure 1.7: The ATLAS detector and the definition of the orthogonal Cartesian coordinate system. Image altered from[23]*

### 1.3.4   Pile-up

Pile-up is the phenomena that several proton-proton collisions occur simultaneously. The number of pile-up is defined as the average number of proton-proton collisions that occur per bunch crossing per second. It is denoted as $\langle\mu\rangle$. $\mu$ can be calculated by adjusting a Poisson distribution to fit the curve created by the number of interactions per bunch crossing at a given luminosity. When this is done $\mu$ will be the mean value of the Poisson distribution. The value of $\mu$ will be higher for after the proposed upgrade compared to now, see section 1.3.6 which may decrease the detector performance.

### 1.3.5   Mono-jet analysis
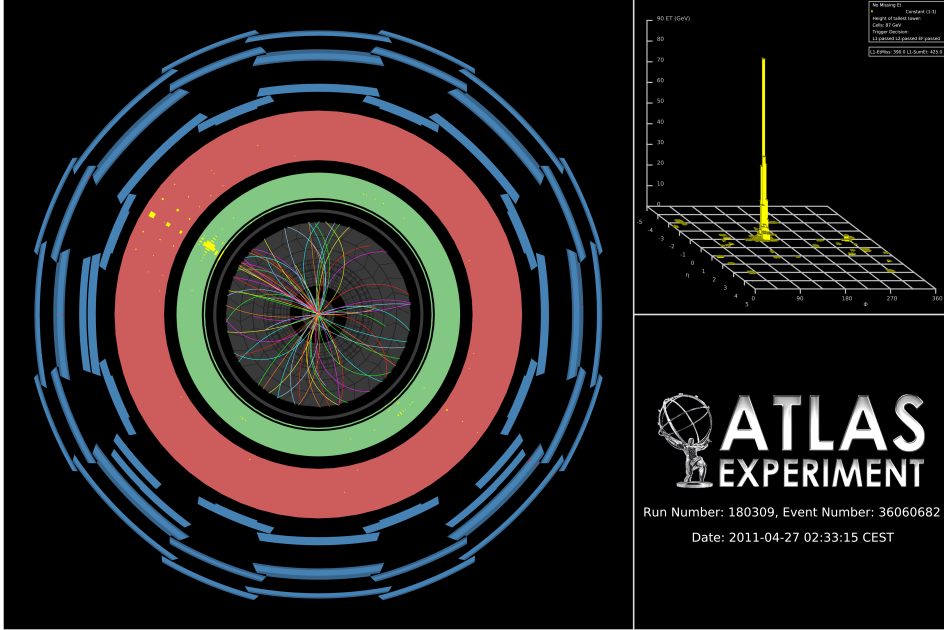


**Figure 1.8:** *Image in the transversal plane of a mono-jet event recorded by the* ATLAS *experiment [24]. The figure in the top right is a diagram in the $(\eta, \phi)$-plane showing where in the calorimeter (red in the main figure) the energy is deposited and how much.*

When measuring the transverse energy one can in some interactions find inconsistencies, such as jets that are in excess in one direction. Conservation of momentum in the transverse plane of the experiment indicates that the sum of all momenta should be zero as before the collision. In figure 1.8 one can see a high energetic jet which gives an excess of transverse energy in one direction after the collision. Since there is no balancing jet there must be transverse energy that is not detected, denoted $E_T^{Miss}$. This gives an indication that the energy to balance this can not be detected. This could for instance be neutrinos or the characteristic signature of WIMPS.

$E_T^{Miss}$ is the modulus of the $E_T^{Miss}$ vector which is defined as:

$$\vec{E_T}^{Miss} = -\sum \vec{p_T}^{Jet} - \sum \vec{p_T}^{Electron} - \sum \vec{p_T}^{Muon} - \sum \vec{p_T}^{Tau} - \sum \vec{p_T}^{Photon} \quad (1.9)$$

where $p_T$ denotes the transverse momenta. There are two main classes of events, signal and background. The signal corresponds to events that would arise from one of the processes in subsection 1.2.5. However to know that the missing energy is sign of the signal then one must understand all the other components that could contribute to the missing energy. Also there must be an excess of missing energy from what is expected from the background.

451 The background comprises of standard model processes that can mimic the mono-
452 jet signature.

### 1.3.6 Phase II high luminosity upgrade

454 At the moment, the whole LHC is undergoing a step by step upgrade program
455 which be finalized around 2022-2023, denoted the high luminosity upgrade, or
456 HL-upgrade. The upgrade consists of different stages, meaning that the upgrade
will halt for periods so that experiments can take place. In figure 1.9 one can see
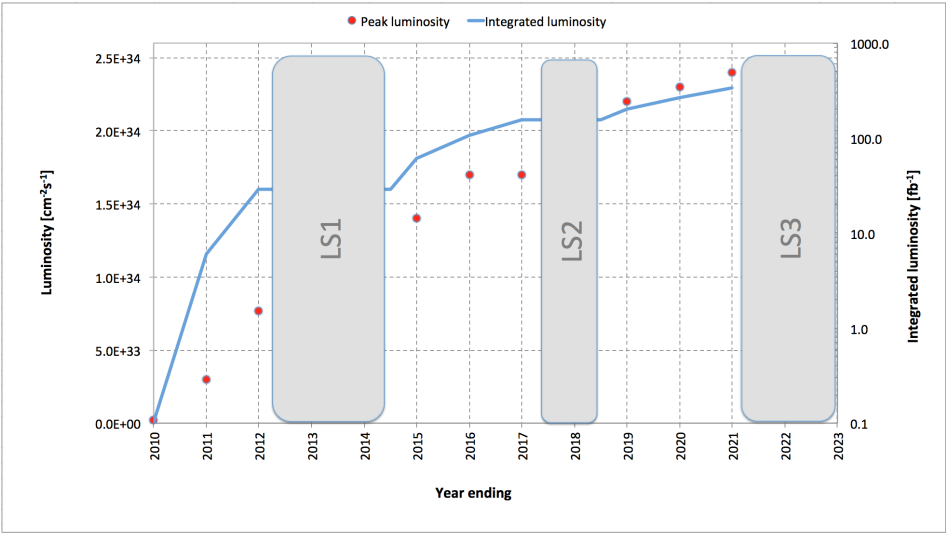


*Figure 1.9: A graph showing the upgrading timetable with the instantaneous luminosity, denoted luminosity, and integrated luminosity expected in the different stages.*

457
458 the three proposed upgrades. The period after LS1 is denoted phase 0, after LS2
459 phase I and after LS3 phase II.

460 LS1  is the upgrade which will take the LHC to its designed performance.

461 LS2  will push the LHC to the ultimate designed instantaneous luminosity with-
462    out too dramatic changes to the accelerator.

463 LS3  which is the focus of this thesis, will increase the instantaneous luminosity
464    even more. Though for this to happen a modification of the whole LHC
465    must be done, instead of just an upgrade and maintenance as before.

466 The following is expected for the experiments done after phase II:

| Entity | Expected | Last run (2012) |
|---|---|---|
| Instantaneous luminosity | $\mathscr{L} \sim 50$ nb$^{-1}$s$^{-1}$ | $\mathscr{L} \sim 10$ nb$^{-1}$s$^{-1}$ |
| Integrated luminosity | $\mathcal{L} = 1000 - 3000$ fb$^{-1}$ | $\mathcal{L} = 20$ fb$^{-1}$ |
| Pile-up | $\langle \mu \rangle = 140$ | $\langle \mu \rangle = 20$ |
| Center of mass energy | $\sqrt{s} = 14$ TeV | $\sqrt{s} = 8$ TeV |

***Table 1.2:*** *Expected running values for the Phase II HL-upgraded LHC with older values for comparison [25].*

Where it should be noted that the integrated luminosity indicates the total amount of data which will be collected after the upgrade is completed before the next upgrade takes place.

### 1.3.7   Monte Carlo simulation

As mentioned before, in this thesis only emulated data has been used. This data is created by using a Monte Carlo (MC) simulation of the background processes and the expected signal. To do this a program called MadGraph is used.

MadGraph [26] starts with Feynman diagrams and then generates simulated events based on lots of different parameters. This generator was used to generate signal samples used in this thesis.

Sherpa, [27] is very similar to MadGraph and was used to generate the background samples used in this thesis.

PYTHIA [28] is a package which adds the correct description of jets to MadGraph by including hadronization. The correct description of pile-up comes from other ATLAS software.

The tool to access all this data and analyse it a tool called ROOT, which is used for programming high energy physics related tools [29].

# 2

# Validation of smearing functions

A full detector simulation of the ATLAS detector based on the GEANT [30] program makes it possible to obtain the expected detector responses to electrons, muons, tau leptons, photons ($\gamma$) and jets of hadrons. However these simulations are extremely time-consuming and require a lot of computing power. Also at the present time only a limited set of these simulations exits for the ATLAS phase II upgrade.

In this thesis a different strategy is used. Instead of performing a full detector simulation the observed particles from the event generator, which simulates the proton-proton collisions, are smeared by using random numbers following resolution functions specific to each type of particle. These emulate how the detector and the reconstruction is affected by the increased luminosity and the pile-up which comes with this.

The resolution functions or smearing functions are the official functions developed from previous studies [1, 31] by the ATLAS collaboration for the study of the ATLAS phase II upgrade. The key feature of those studies was that the direction of the momenta is unaffected and that only jets and $E_T^{Miss}$ are affected by pile-up. Since this was confirmed in previous studies it was not incorporated into the smearing functions as discussed more in section 2.1.

Since part of this thesis work is to take the official ATLAS smearing functions and apply the smearing to each particle, it is important to check that the energy and momenta resolutions of the smeared objects are consistent with the expected values. Thus in this chapter the energy and momenta resolutions are measured after applying the smearing to some simulated processes and the resulting resolutions are compared with the expected values.

## 2.1   Smearing functions

In a simulation of a proton-proton collision all quantities such as energy, momentum and direction of all produced particles are perfectly known. In a real experiment it is only possible to get measured values from the detector. The detector energy and momentum resolutions given in the smearing functions relate the measured values are to the true values on a statistical basis. To emulate the measured energies and momenta, their true values are smeared using the known detector resolutions.

These smearing functions are designed so that they take into account the efficiency of the different detectors, limitations from how they are constructed as well as their dependence on pile-up. They also take into account how all this varies depending on the measured entries energy or momenta.

Terminology:

- Data before smearing, simulated data, is denoted as data at a truth level or truth data.

- Data after smearing, which is comparable to what is measured is denoted as reconstructed or reco data.

### 2.1.1   Electron and photon

The identification of electrons relies on finding an isolated electron track and a pattern in the calorimeter compatible with an electron shower. Pile-up will affect the electrons by decreasing the efficiency to identify an electron because of the increased number of tracks. However for the identified electrons the energy resolution will be close to that without pile-up.

The electron and photon have the same smearing since they are both detected in a similar way.

### 2.1.2   Muon

The identification of muons relies on isolated tracks in the inner detector being matched with information in the muon system. Since the muon system is the outer most detector seen from the collision point it is unaffected by the false detection effects of pile-up.

### 2.1.3   Tau

Tau is detected similarly to electron and photon. In this thesis all tau processes are for simplicity assumed to be at 3 prong. Where prong refers to the different amount of tracks from which they were reconstructed. This in turn means that the effect of pile-up will be worse compared to an electron as a triplet must be found in an increased number of tracks.

### 2.1.4   **Jets**

The largest effect of pile-up is to add additional jets in the ATLAS detector. These additional jets contribute to additional energy deposited inside the existing jets and to $E_T^{Miss}$.

### 2.1.5   **Missing Transversal Energy**

$E_T^{Miss}$, the missing transversal energy, which was discussed in subsection 1.3.5, and defined in (1.9) is calculated by knowing that there should be energy conservation in the collision. In is comprised of different parts, one from neutrinos, one from errors in the other measurements and one from new physics. It should be affected by pile-up as described above.

## 2.2   **Validation**

To validate the smearing functions a comparison with Ref. [31] was made where the standard deviation, depending on the energy of momentum value of an entity, was given, see section 2.4. This is performed using the simulated processes listed in table 2.1.

*Table 2.1: Different processes from where data has been taken. Each sample is a simulation of a physical process, the simulation names can be found in appendix A*

| Particle | Process |
|----------|---------|
| Electron | W→ $e\nu$ |
| Muon | W→ $\mu\nu$ |
| Tau | W→ $\tau\nu$ |
| $\gamma$ | $\gamma$ + Jet sample |
| Jets | Jet sample |
| $E_T^{Miss}$ | Z→ $\nu\nu$ + Jet sample |

### 2.2.1   **Method**

The energy and momentum resolutions are obtained for each type of particle by comparing the values before and after smearing.

This is done by looking at the reco data for a given value of truth energy or momentum value denoted as taking a slice. Since the smearing functions takes a lot into account the match will not be a fine line as seen in figure 2.3b.

By fitting a Gaussian curve to this data will then result in the standard deviation which is used in the validation. The standard deviation is also known as the resolution of the data and will be denoted $\sigma$ and not cross-section as in chapter 1

This resolution is then compared to previous results, [31].

To get enough statistics enough data must be available for a given truth energy or momenta and the analysis must be specific enough to only look at a narrow enough interval around this point.

Step by step method

- Take a MC sample with a given particle, i.e electrons.

- Choose a slice of electron which have a truth energy of a given value (75 GeV for electrons).

- Plot the smeared electron energy for this slice of truth energy. Given for electrons and photons in figure 2.1.

- For this distribution of smeared energy, fit a Gaussian distribution and calculate the sigma value of this Gaussian.

- Compare this sigma, which is the calculated resolution to the expected resolution given from the smearing functions.

## 2.3   **Results**

As discussed above, the method was to plot the data against its smeared counterpart and through this determine $\sigma$ to see if it conforms to the expected values.

Only one energy or momenta value is shown for simplicity, though the comparison was done for different energy values. The energy is denoted E and in the figures momenta is denoted $P_T$ for transversal momenta.

The average number of pile-up, explained in subsection 1.3.4, is fixed at 60 as a benchmark unless anything else is stated.

As the comparison, figure 2.4, figure 2.1, figure 2.2 and figure 2.5 are divided depending on the different $\eta$ values.

All results are summarized in table 2.5.

<sub>595</sub> ## 2.3.1   Electron and photon

<sub>596</sub> Since these interact very similarly in the detector, their smearing functions are
<sub>597</sub> identical. The slice value represents at which value of unsmeared energy or mo-
<sub>598</sub> mentum this smearing occurs.
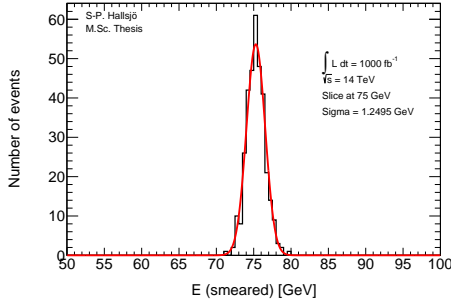


*(a)* Electron energy after smearing for $|\eta| <$ 1.4.
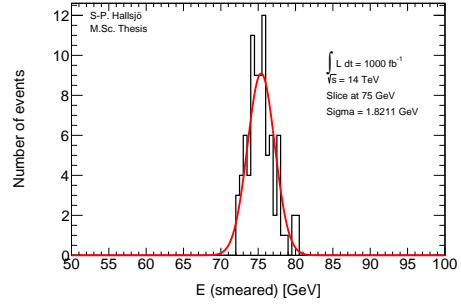


*(b)* Electron energy after smearing for $1.4 < |\eta| < 2.47$.
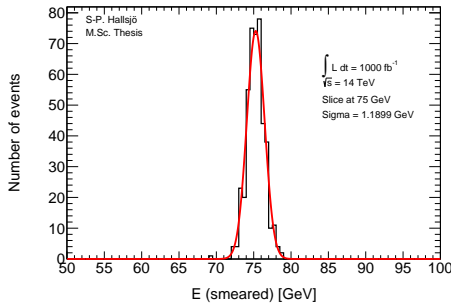


*(c)* Photon energy after smearing for $|\eta| <$ 1.4.
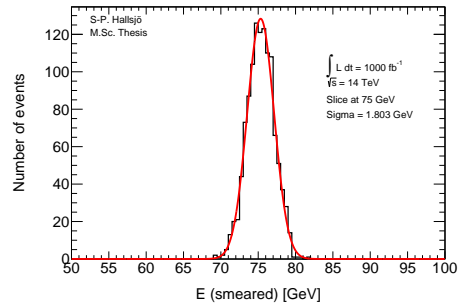


*(d)* Photon energy after smearing for $1.4 < |\eta| < 2.47$.

**Figure 2.1:** *Photon and electron energy after smearing.*

599  ### 2.3.2   Muon

600  Since muons are shielded from the effects of pile-up only efficiency and detector
601  limitations affect the smearing.
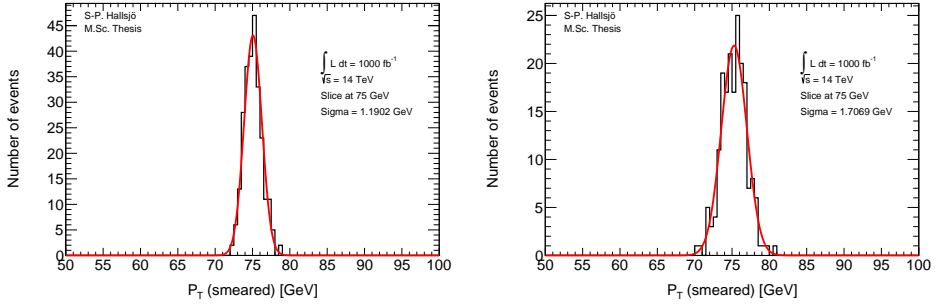


**(a)** *Muon momenta after smearing for $|\eta| <$ 1.05.*  **(b)** *Muon momenta after smearing for $1.05 < |\eta|$.*

**Figure 2.2:** *Muon momenta after smearing.*

602  ### 2.3.3   Tau

603  As described in subsection 2.1.3 tauons are detected similarly to electrons and
604  photons. Thus the plots should look similarly to those in the previous subsection
605  apart from the slice being at 150 GeV. In figure 2.3a the Gaussian fit (red) and the
606  data (black) are given for tau detected through 3 prong. In figure 2.3b smeared
607  verses truth energy is shown.
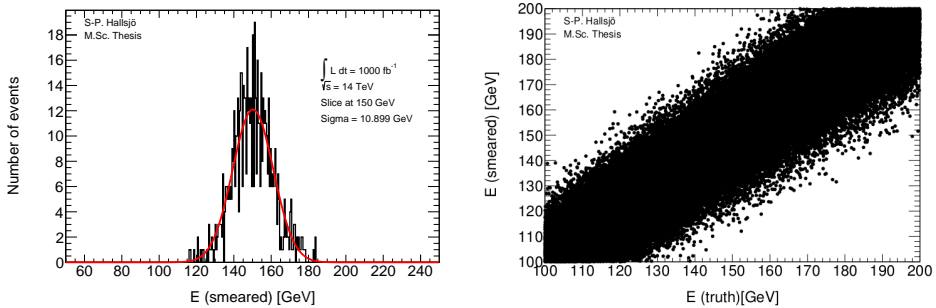


**(a)** *Tau energy after smearing.*   **(b)** *Tau energy vs smeared.*

**Figure 2.3:** *Tau energy after smearing and energy vs smearing.*

### 2.3.4   **Jets**

Jets as described in subsection 1.3.5, are hadronic showers. The smearing functions are divided into four different regions depending on the angle $\eta$.
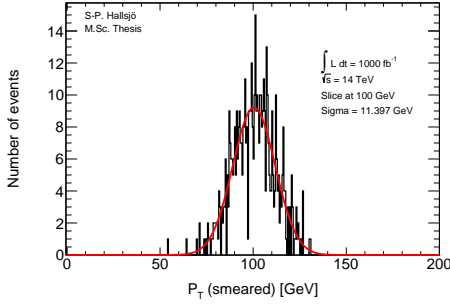


*(a)* Jet momenta after smearing
for $|\eta| < 0.8$.
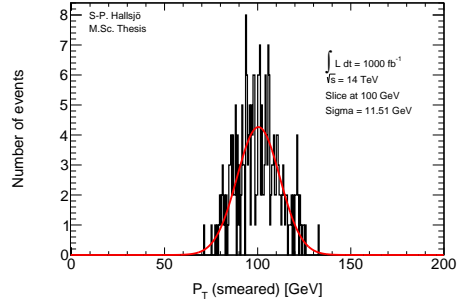


*(b)* For $0.8 < |\eta| < 1.2$.
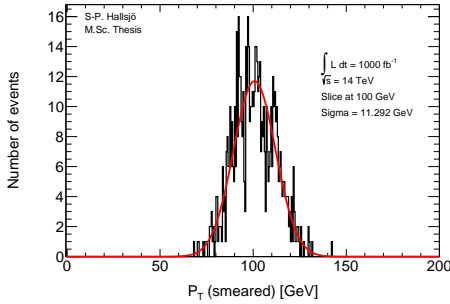


*(c)* Jet momenta after smearing
for $1.2 < |\eta| < 2.8$.
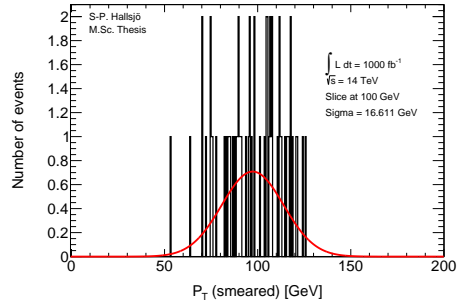


*(d)* For $2.8 < |\eta| < 3.6$. Very odd due to the
low amount of available data.
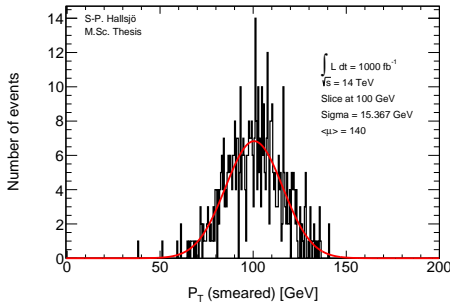


*(e)* Jet momenta after smearing
for $|\eta| < 0.8$ at $\langle \mu \rangle = 140$.
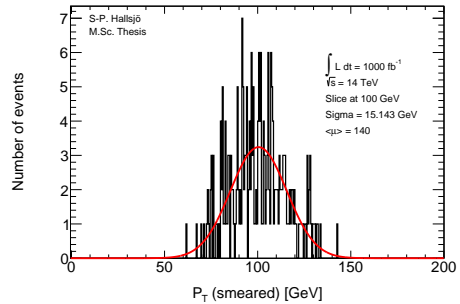


*(f)* For $0.8 < |\eta| < 1.2$ at $\langle \mu \rangle = 140$.

**Figure 2.4:** *Jet momenta after smearing.*

⁶¹¹ Where $\langle \mu \rangle$ is the average number of simultaneous proton-proton collisions as
⁶¹² explained in subsection 1.3.4.

### ⁶¹³ 2.3.5 Missing Transversal Energy

⁶¹⁴ The figures in this subsection are, compared to the above, given as absolute smear-
⁶¹⁵ ing, thus at 0 it represents that the energy is unsmeared, compared to the others
⁶¹⁶ where the slice value represents the unsmeared.

⁶¹⁷ Here the $E_T^{Miss}$ is projected down to the x- and y-axis, since these are the transver-
⁶¹⁸ sal axes, to be smeared.
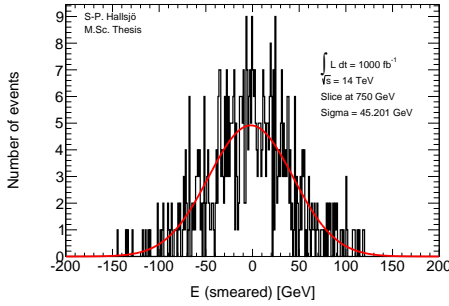


(a) $E_T^{Miss}$ smearing along the x-axis.
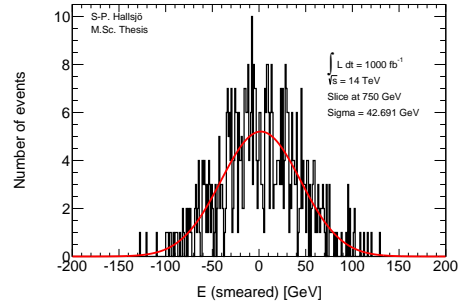


(b) $E_T^{Miss}$ smearing along the y-axis.
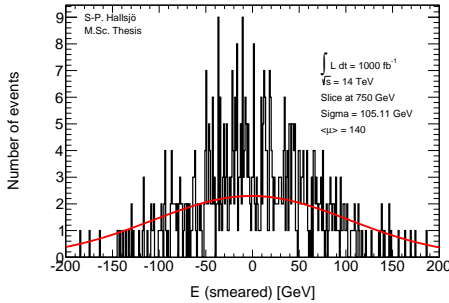


(c) $E_T^{Miss}$ smearing along the y-axis for $\langle \mu \rangle = 140$.

**Figure 2.5:** $E_T^{Miss}$ smearing plots

## 2.4   Expected results

Since the leptons and photons are all detected by fitting detectors responses to different tracks, meaning that the effect of pile-up should be that there are more track to match, but it should not affect which ones are matched. The independence of pile-up for leptons and photons is backed up in previous research, for instance [1, 32].

To validate the smearing code, comparisons are made with [31] which gave the following formulation for the expected $\sigma$:

| Observable | Absolute $\sigma$ |
|---|---|
| Electron & photon | $\sigma = 0.3 \oplus 0.1\sqrt{E(GeV)} \oplus 0.01E(GeV), |\eta| < 1.4$ |
| | $\sigma = 0.3 \oplus 0.15\sqrt{E(GeV)} \oplus 0.015E(GeV), 1.4 < |\eta| < 2.47$ |
| Muon momentum | $\sigma = \frac{\sigma_{id}\sigma_{ms}}{\sigma_{id}\oplus\sigma_{ms}}$ |
| | $\sigma_{id} = p_T(a_1 \oplus a_2 p_T)$ |
| | $\sigma_{ms} = p_T(\frac{b_0}{p_T} \oplus b_1 \oplus b_2 p_T)$ |
| Tau energy | $\sigma = (0.03 \oplus \frac{0.76}{\sqrt{E(GeV)}})E(GeV)$, for 3 prong. |
| Jet momentum | $\sigma = p_T(GeV)(\frac{N}{p_T} \oplus \frac{S}{\sqrt{p_T}} \oplus C)$ |
| | where $N = a(\eta) + b(\eta)\mu$ |
| $E_T^{Miss}$ | $\sigma = (0.4 + 0.09\sqrt{\mu})\sqrt{\sum E(GeV) + 20\mu}$ |

**Table 2.2:** *Expected absolute $\sigma$ where the parameters are given for muons in table 2.3 and for jets in table 2.4. Functions take from [31].*

| | $a_1$ | $a_2$ | $b_0$ | $b_1$ | $b_2$ |
|---|---|---|---|---|---|
| $|\eta| < 1.05$ | 0.01607 | 0.000307 | 0.24 | 0.02676 | 0.00012 |
| $|\eta| > 1.05$ | 0.03000 | 0.000387 | 0.00 | 0.03880 | 0.00016 |

**Table 2.3:** *Parameters used in the muon smearing function taken from [31].*

| $|\eta|$ | a | b | S | C |
|---------|-----|------|------|------|
| 0-0.8   | 3.2 | 0.07 | 0.74 | 0.05 |
| 0.8-1.2 | 3.0 | 0.07 | 0.81 | 0.05 |
| 1.2-2.8 | 3.3 | 0.08 | 0.54 | 0.05 |
| 2.8-3.6 | 2.8 | 0.11 | 0.83 | 0.05 |

*Table 2.4: Parameters used in the jet smearing function taken from [31].*

| Process | $\sigma$ [GeV] | Expected $\sigma$ |
|---------|----------------|-------------------|
| Electron low $\eta$ | $1.25 \pm 0.05$ | 1.18 |
| High $\eta$ | $1.82 \pm 0.14$ | 1.74 |
| Photon low $\eta$ | $1.19 \pm 0.04$ | 1.18 |
| High $\eta$ | $1.80 \pm 0.04$ | 1.74 |
| Muon low $\eta$ | $1.19 \pm 0.05$ | 1.50 |
| High $\eta$ | $1.71 \pm 0.09$ | 2.18 |
| Tau | $10.90 \pm 0.31$ | 10.34 |
| Jet low $\eta$ | $11.40 \pm 0.35$ | 11.60 |
| $\langle \mu \rangle = 140$ | $15.37 \pm 0.47$ | 15.77 |
| Mid low $\eta$ | $11.51 \pm 0.52$ | 11.94 |
| $\langle \mu \rangle = 140$ | $15.14 \pm 0.68$ | 15.95 |
| Mid high $\eta$ | $11.29 \pm 0.31$ | 10.94 |
| High $\eta$ | $16.61 \pm 1.53$ | 13.50 |
| $E_T^{Miss}$x−axis | $45.20 \pm 1.35$ | 48.45 |
| $E_T^{Miss}$y−axis | $42.69 \pm 2.28$ | 48.45 |
| $\langle \mu \rangle = 140$ | $105.11 \pm 12.24$ | 87.28 |

*Table 2.5: $\sigma$ values.*

- Where the given $\sigma$ is still the absolute.

- Where the large difference between calculated and expected $\sigma$ for Muons and $E_T^{Miss}$ is explained by to optimistically calculated errors in $\sigma$.

## 2.5    Discussion

### 2.5.1    Smearing independent on pile-up

From the validation done it is interesting to note that the smearing functions were created from previous studies, [1, 32], which had shown that leptons and photons are not affected by pile-up. This may seem incredible however it becomes quite logical when one understands how the detectors work. To be able to detect particles the detectors must detect an excess of energy which comes from a particle passing through. This should not be distorted by an increased pile-up. The amount of particles passing through will of course increase, but the detections should be unaffected as well as the recreation of the events. However with the same logic it makes sense that jets and $E_T^{Miss}$ are quite affected since they are combined of several parts, either hadronic particles or by all the transversal missing energy.

Another interesting part is how the effect diminishes with an increasing energy. As seen above, and through the the formulas in table 2.2, for the high energies which are of interest here the effect of pile-up minimal.

### 2.5.2    Comparison to expected results

One of the major problems in the comparison was to get the significance of the Gaussian fit to be calculated correctly. The tool ROOT has a lot of different features which made this task somewhat difficult. Also since this is a statistical property there is a statistical fluctuation in the result.

Another was to retrieve the correct values from the paper, [31], since it was unclear if the values given were absolute or scale dependent. This has now been corrected in a new version of the paper.

## 2.6 Conclusion

The smearing functions work as intended within 5.8 sigma, however when using a test box and averaging the sigmas one ends up with half of this for the extreme cases, muons and $E_T^{Miss}$y−axis.

# 3

## Evaluating dark matter signals

The main goal of the thesis is to investigate if certain dark matter signals can be detected after the high luminosity upgrade. One immediate worry is that the background will be large in comparison to the signal, making the signal undetectable.

Another goal is to investigate if it might become more difficult to differentiate between the signal and background due to the degradation of jet and missing energy resolutions in the high luminosity upgrade.

This thesis focus on using a luminosity at $1000$ fb$^{-1}$ and a center of mass energy at 14 TeV. The reco data is created using a pile-up rate, $\langle \mu \rangle = 140$ as expected during phase II.

The signal models are given in appendix A along with the background models. The different models were introduced subsection 1.2.5 and will be discussed in more detail in this chapter.

Each signal model has been evaluated in different signal regions and the detectability has been evaluated using a statistical p-value.

# 3.1  Signal to background ratio

## 3.1.1  Signal Region

A signal region (SR) is defined as a set of selections on event variables designed to create a sample which is enriched in signal and depleted of background. One usually tries to design the signal region so that the signal is large enough and the background small enough that one would statistically be able to either:

- Exclude the signal if the observation of the data is compatible with a background only hypothesis.

- Detect the signal and quantify the significance of the excess in data over background if the data is consistent with a signal + background hypothesis.

An event is a recorded proton-proton collision which consists of hundreds or thousands of observables such as the number of electrons, muons, jets, tau leptons, gammas or $E_T^{Miss}$ each with their energy and momenta.

To define an optimal signal region is not known a priori and has to be studied for different signal models. The optimal region typically changes e.g with a change of the mass of new particles for instance the WIMP mass or the suppression scale. This is why there are several different signal regions to be studied in this thesis.

## 3.1.2  Weight

A weight is used to normalize different types of data so that they can be compared. As given in (1.7), the total number of events can be estimated as:

$$N = \sigma \int \mathscr{L} \, dt \equiv \sigma \mathcal{L} \tag{3.1}$$

Thus, if all events are generated at different luminosities, depending on the computing power of the computer which performed the simulation, the following weight should be used to receive the events at a new luminosity:

$$weight = \frac{\mathcal{L}\sigma}{N_{Raw}} \tag{3.2}$$

where $N_{Raw}$ is the number of events expected at the luminosity that was set to create the data, compared to $\mathcal{L}$ which is the luminosity at which the data is compared and $\sigma$ is the cross-section. In this thesis the luminosity is fixed at $\mathcal{L} = 1000\text{fb}^{-1}$.

## 3.1.3  Verification of background normalization

To verify that the background samples are correctly normalized they are compared with Ref. [33] in which the center of mass energy is 8 TeV and the luminosity is 10 fb$^{-1}$. Since the luminosity is not 1000 fb$^{-1}$ as used in this thesis the expected values from the paper scaled up with a factor 100 to be comparable.

Somewhat unexpectedly a center of mass energy at 8 TeV had cross-sections a factor 4 lower than the cross-sections at 14 TeV. These cross-sections are generated

either with MadGraph[26] or PYTHIA[28] depending on the generator given for
each dataset in appendix A.

The signal regions used in the article were the following:

| Selection Criteria | | |
|---|---|---|
| Jet veto, require no more than 2 jets with $p_T > 30 GeV$ and $|\eta| < 4.5$ | | |
| Lepton veto, no electron or muon | | |
| Leading jet with $|\eta| < 2.0$ and $\Delta\phi(jet, E_T^{Miss}) > 0.5$ (second-leading jet) | | |
| signal region | SR3p | SR4p |
| minimum leading jet $p_T$ (GeV) | 350 | 500 |
| minimum $E_T^{Miss}$ (GeV) | 350 | 500 |

*Table 3.1: The signal regions from Ref. [33].*

The article [33] has in total four signal regions, unfortunately since the simulated
events used in this thesis are filtered before the analysis only the two highest
regions are comparable. This can be seen in table 3.3 in subsection 3.4.1.

### 3.1.4   Errors in data

To make a through analysis of the background it is important to take into con-
sideration different errors that exist in the number of events. This is especially
important when looking at which signals can be excluded in different signal re-
gions. There exists three main types of errors:

- Statistical errors from MC.

- Statistical errors from the control region.

- Systematic errors.

The statistical errors from MC come from the method of generating background
events and is unfortunately nothing that can be estimated when one is not gener-
ating the events.

The statistical errors from the control region require an explanation of what a
control region is. A control region (CR) is similar to a signal region, a set of
criteria which are imposed on the data. This criteria are set so that there can
be a region with almost no signal. In this CR there will still be fluctuations in
the amount of background events due to statistical effects, which can then be
measured.

The systematic errors is a fixed error which is always present coming from differ-
ent approximations in how all the events were generated.

### 3.1.5   Figure of merit

To be able to evaluate different signal regions and different signal models, a figure
of merit p is used. The value p is the probability for the background to fluctuate

736 to the value of the signal + background. Thus if the p-value is small, regardless
737 if the signal is large or the background or its fluctuations are small, it is improb-
738 able that the background could result in the same value as if there was a signal
739 and background. This means that for a sufficiently small p-value the signal is
740 detectable.

741 Assuming the expected number of background events are B $\pm\sigma_B$ where $\sigma_B$ is the
742 quadratic sum of the statistical error from Monte Carlo, the statistical error from
743 the control region (CR) and the systematic errors as explained in subsection 3.1.5.
744 The expected number of signal events is S, assumed without fluctuation.

745 If no uncertainty in B or S is assumed, then the probability that the background
746 will fluctuate up to the signal and background should follow a Poisson distribu-
747 tion as such:

$$P(S+B|B) = \frac{e^{-B}B^{(S+B)}}{(S+B)!} \tag{3.3}$$

748 The probability that the background will fluctuate to a value N larger or equal to
749 the signal and background then becomes:

$$P(B{\geq}S+B|B) \equiv P(N|B) = \sum_{N=S+B}^{\infty} \frac{e^{-B}B^N}{N!} \tag{3.4}$$

750 However since there is an uncertainty in the background, the probability distri-
751 bution P(N|B) must be convoluted with a Gaussian function:

$$G(N_B|B,\sigma_B) = \frac{1}{\sigma_B\sqrt{2\pi}}e^{-\frac{(N_B-B)^2}{2\sigma_B^2}} \tag{3.5}$$

where $N_B$ is the expected number of background events. The convolution is done
using $N_B$ as B resulting in the total probability density function:

$$F(N|N_B, \sigma_B) = P(N|B)*G(N_B|B,\sigma_B) =$$
$$= \int_{-\infty}^{\infty} P(N|N_B - B)G(N_B|B, \sigma_B)dN_B \tag{3.6}$$

752 Inserting the sum over N leads to the probability of the background fluctuation
753 to signal and background being obtained as.

$$p = \sum_{N=S+B}^{\infty}\int_{-\infty}^{\infty} P(N|N_B{-}B)G(N_B|B,\sigma_B)dN_B \tag{3.7}$$

In this thesis, two different models of the error in the background $\sigma_B$ are used.
Both models are based on Ref. [33]. As described in the beginning of this subsec-
tion the error is calculated as:

$\sigma_B$ = Statistical error from MC $\oplus$ Statistical error in CR $\oplus$ Systematic error

754   • The statistical error from MC has been neglected since there is no way of
755     estimating it.

756   • The statistical error from background CR has been take from the article and
757     assumed to decrease with the increased luminosity as, $\frac{30}{380}\frac{\sqrt{L_{old}}}{\sqrt{L_{new}}}$

758   • The systematic error has been given two different values, from the article:
759     $\frac{30}{380}$ or fixed at 0.02.

760   • All this results the total error being used as either, 0.08 or 0.02.

## 3.1.6   D5 operator models

762   As described in subsection 1.2.5, one of the signals is modelled using the D5
763   operator. In this thesis two different scenarios are used, one at a dark matter
764   mass of 50 GeV and one at 400 GeV.

765   Each of these models are modelled with a mass suppression scale, denoted M⋆,
766   which is connected to the cross-section of the process through:

$$\sigma_{new} = \frac{\sigma_{old}}{M^{\star}} \tag{3.8}$$

767   where $\sigma_{old}$ is the theoretically calculated sigma and $\sigma_{new}$ denotes the sigma which
768   is used taking the mass suppression scale into account. In subsection 3.4.3 it is
769   determined which values of M⋆ could be excluded with the upgraded LHC phase
770   2 upgrade and ATLAS.

## 3.1.7   Light vector mediator models

772   As described in subsection 1.2.5, the other signal model is a vector mediator
773   model. In this thesis these signals have two different width scenarios and a num-
774   ber of different mediator mass scenarios. **Where width is related to the lifetime**
775   **of the dark matter particle.** In addition to this there are, as with the D5 operator,
776   two different dark matter masses, one at 50 GeV and one at 400 GeV.

777   The result of the investigation of which models are excludable with the upgraded
778   LHC phase 2 upgrade and ATLAS are given in subsection 3.4.4.

## 3.2   Signal region definitions

### 3.2.1   Signal regions

To be able to compare signal results to previous studies new signal regions were devised. It was also discovered that the requirement of no electrons or muons was to harsh for the signal models. Through this these new selection criteria were devised. In table 3.2 the superscript lead denotes the the entity with highest transversal momentum $p_T$. Thus $electron^{lead}$ would be the simulated electron in an event with the highest $p_T$.

| Selection Criteria |
|---|
| Jet veto, require no more than 2 jets with $p_T > 30 GeV$ and $|\eta| < 4.5$ |
| Lepton veto, no electron or muon. |
| The electron veto is defined: $\Delta R(jet^{lead}, electron^{lead}) \geq 0.4$ and $electron^{lead} p_T > 20 GeV$ removed. |
| The muon veto is defined: $\Delta R(jet^{lead}, muon^{lead}) \geq 0.4$ and $muon^{lead} p_T > 20 GeV$ removed. |
| Leading jet with $|\eta| < 2.0$ and $\Delta\phi(jet, E_T^{Miss}) > 0.5$ (second-leading jet) |

| signal region | SR1 | SR1p | SR2 | SR3 | SR4 |
|---|---|---|---|---|---|
| minimum leading jet $p_T$ (GeV) | 350 | 500 | 600 | 800 | 1000 |
| minimum $E_T^{Miss}$ (GeV) | 350 | 500 | 600 | 800 | 1000 |

| signal region | SRa | SRb | SRc | SRd |
|---|---|---|---|---|
| minimum leading jet $p_T$ (GeV) | 350 | 350 | 350 | 350 |
| minimum $E_T^{Miss}$ (GeV) | 350 | 600 | 800 | 1000 |

***Table 3.2:*** *The new signal regions.*

### 3.2.2   Verifying background data

To make sure that the altered electron veto still produces results comparable with [33] a comparison is made again. This can be seen in subsection 3.4.1 in table 3.4.

## 3.3   Mitigating the effect of the high luminosity

As discussed in subsection 2.5.1 the smearing functions effect of pile-up should be minimal in the high energy regions which are of interest in this thesis.

From the formulation of the smearing functions, the biggest effect should be seen at low energies. This is related to the difficulty for the hardware triggers to select events. This means that one drawback of the high luminosity upgrade is that very low energy signal regions will be lost.

The effect of the high luminosity is seen in chapter 3.4 and discussed in subsection 3.5.2.

## 3.4   Results

### 3.4.1   Verifying background data

In table 3.3 and table 3.4 a comparison has been made between the number of simulated background events at a truth level and the number of expected events by scaling up the values from Ref. [33] by a factor 100. Truth data was used to not let the increased pile-up value affect the comparison. It can be seen that the simulated events and expected events coincide quite well on all accounts apart from W$\to \tau\nu$, W$\to \mu\nu$ and thus the total as well.

The difference in W$\to \tau\nu$ can be explained by the fact that $\tau$ can not be recreated as a jet in the simulated events which it can in measured events.

The difference in W$\to \mu\nu$ is explained through the simulated events having a better separation of muons neutrinos and E$_T^{Miss}$.

|  | SR3p | | SR4p | |
|---|---|---|---|---|
| Process | Simulated | From paper | Simulated | From paper |
| Z$\to \nu\nu$ | 140298 | 152000 | 25250 | 27000 |
| W$\to \tau\nu$ | 40701 | 37000 | 5862 | 3900 |
| W$\to e\nu$ | 11229 | 11200 | 1507 | 1600 |
| W$\to \mu\nu$ | 13727 | 15800 | 1872 | 4200 |
| Total background | 205955 | 218000 | 34491 | 36700 |

**Table 3.3:** *Comparison of the simulated and expected events from Ref. [33] with $\mathcal{L} = 1000 fb^{-1}$, cross-sections corresponding to $\sqrt{s} = 8 TeV$ and using the same electron and muon veto.*

|  | SR1 | | SR1p | |
|---|---|---|---|---|
| Process | Simulated | From paper | Simulated | From paper |
| Z$\to \nu\nu$ | 150753 | 152000 | 27569 | 27000 |
| W$\to \tau\nu$ | 49320 | 37000 | 7318 | 3900 |
| W$\to e\nu$ | 18329 | 11200 | 2534 | 1600 |
| W$\to \mu\nu$ | 22290 | 15800 | 3218 | 4200 |
| Total background | 240690 | 218000 | 40639 | 36700 |

**Table 3.4:** *Comparison of the simulated and expected events from Ref. [33] with $\mathcal{L} = 1000 fb^{-1}$, cross-sections corresponding to $\sqrt{s} = 8 TeV$ and using a modified electron and muon veto.*

### 3.4.2   Events

In the following tables the number of events are given using one of the D5 operators as the signal, and the background in the different signal regions. The number of background events is also used for the vector mediator signals.

| Process at $\sqrt{s}$ = 14TeV | SR1 | SR2 | SR3 | SR4 | SRa | Srb | Src | Srd |
|---|---|---|---|---|---|---|---|---|
| D5, mDm=50 GeV, M*=1TeV | 131844 | 30900 | 11053 | 4532 | 131844 | 37217 | 13280 | 5387 |
| Z→ νν | 619752 | 44146 | 8764 | 2205 | 619752 | 61193 | 11975 | 2998 |
| W→ τν | 169983 | 8753 | 1479 | 344 | 169983 | 12047 | 2032 | 453 |
| W→ eν | 63026 | 2986 | 510 | 114 | 63026 | 4114 | 688 | 160 |
| W→ μν | 76618 | 3880 | 658 | 162 | 76618 | 5094 | 871 | 199 |
| Total background | 929379 | 59765 | 11411 | 2825 | 929379 | 82448 | 15566 | 3810 |

*Table 3.5: Signal and background events for truth data in the signal regions.*

| Process at $\sqrt{s}$ = 14TeV | SR1 | SR2 | SR3 | SR4 | SRa | SRb | SRc | SRd |
|---|---|---|---|---|---|---|---|---|
| D5, mDm=50 Gev, M*=1TeV | 122117 | 28663 | 10273 | 4259 | 122117 | 39618 | 14151 | 5679 |
| Z→ νν | 568410 | 40518 | 8012 | 2023 | 568410 | 74564 | 13817 | 3318 |
| W→ τν | 170999 | 8644 | 1442 | 314 | 170999 | 16241 | 2446 | 536 |
| W→ eν | 60071 | 2799 | 470 | 110 | 60071 | 5366 | 835 | 183 |
| W→ μν | 73495 | 3704 | 629 | 152 | 73495 | 6622 | 1046 | 236 |
| Total background | 872975 | 55665 | 10552 | 2599 | 872975 | 102793 | 18144 | 4273 |

*Table 3.6: Signal and background events for reco data with $\langle \mu \rangle$ = 140 in the signal regions.*

Note how the ratio between the number of signal events and total background increases from the first to the last signal regions meaning that these are good choices of signal regions. Also note how similar the two tables are even though table 3.6 is at reco with a pile-up rate of 140.

<sup>818</sup> ### 3.4.3  Limit on M\*

<sup>819</sup> For the D5 operators as described in subsection 3.1.6 limits on the mass suppres-
<sup>820</sup> sion has been calculated by evaluating at which point the signal is covered by
<sup>821</sup> the background, meaning that the p-value > 0.05. This is done using the two
<sup>822</sup> different error models as described in subsection 3.1.5 as figures of merit.

<sup>823</sup> The limit is found, seen as a horizontal line in both figure 3.1 and figure 3.2, when
<sup>824</sup> the p-value = 0.05. In these images the effect of a change of error model can be
<sup>825</sup> seen as a left shift but no change in incline.



*(a)*                                    *(b)*
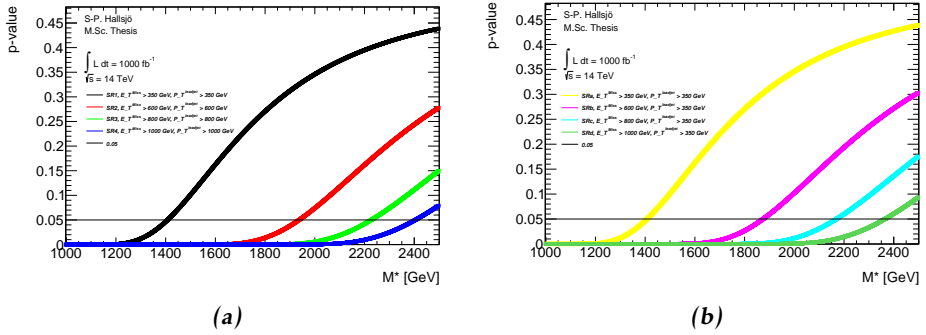
**Figure 3.1:** *Limits of the mass suppression on a truth level for error model 0.02.*



*(a)*                                    *(b)*
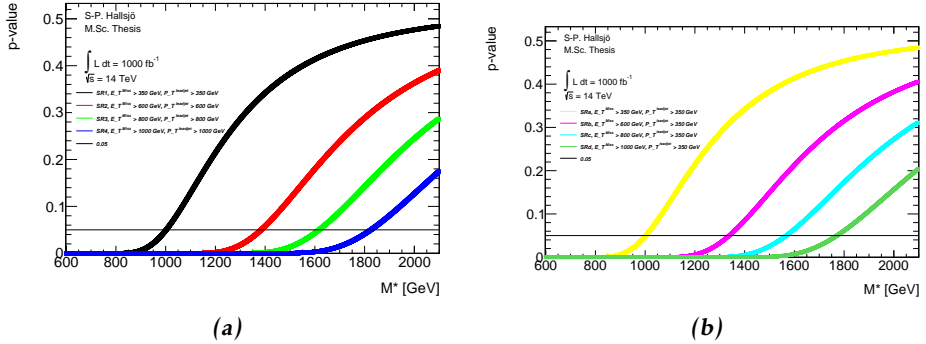
**Figure 3.2:** *Limits of the mass suppression on a truth level for error model 0.08.*

<sup>826</sup> Calculating the instersection between these lines and 0.05 results in, tables 3.7-
<sup>827</sup> 3.10 for both a dark matter mass of 50 GeV and at 400 GeV at the different error
<sup>828</sup> models.

| Signal region | Truth [GeV] | Reco [GeV] |
|---|---|---|
| SR1, symmetric 350 GeV | 1407 | 1402 |
| SR2, 600 | 1936 | 1934 |
| SR3, 800 | 2227 | 2226 |
| SR4, 1000 | 2404 | 2406 |
| SRa, symmetric 350 GeV | 1425 | 1421 |
| SRb, asymmetric 600 GeV | 1874 | 1803 |
| SRc, 800 | 2169 | 2125 |
| SRd, 1000 | 2365 | 2340 |

**Table 3.7:** *Limits on mass suppression scales in GeV given for mDm=50 GeV and the 0.02 error model.*

| Signal region | Truth [GeV] | Reco [GeV] |
|---|---|---|
| SR1 | 1002 | 999 |
| SR2 | 1384 | 1382 |
| SR3 | 1617 | 1619 |
| SR4 | 1825 | 1834 |
| SRa | 1338 | 1286 |
| SRb | 1356 | 1303 |
| SRc | 1567 | 1533 |
| SRd | 1771 | 1745 |

**Table 3.8:** *Limits on mass suppression scales in GeV given for mDm=50 GeV and the 0.08 error model.*

| Signal region | Truth [GeV] | Reco [GeV] |
|---|---|---|
| SR1, symmetric 350 Gev | 1333 | 1329 |
| SR2, 600 | 18481 | 1847 |
| SR3, 800 | 2162 | 2163 |
| SR4, 1000 | 2332 | 2303 |
| SRa, symmetric 350 Gev | 1350 | 1346 |
| SRb, asymmetric 600 Gev | 1789 | 1721 |
| SRc, 800 | 2106 | 2059 |
| SRd, 1000 | 2288 | 2258 |

**Table 3.9:** *Limits on mass suppression scales in GeV given for mDm=400 GeV and the 0.02 error model.*

What should be noted from these tables is the significant difference between the different signals regions, especially between 4 and d which are similar apart from the lead jet momenta cut. Also how small the effect from pile-up seems to be and the increase in dark matter mass.

| Signal region | Truth [GeV] | Reco [GeV] |
|---------------|-------------|------------|
| SR1 | 949 | 946 |
| SR2 | 1321 | 1320 |
| SR3 | 1570 | 1573 |
| SR4 | 1770 | 1755 |
| SRa | 961 | 959 |
| SRb | 1277 | 1228 |
| SRc | 1521 | 1484 |
| SRd | 1714 | 1684 |

**Table 3.10:** *Limits on mass suppression scales in GeV given for mDm=400 GeV and the 0.08 error model.*

### 3.4.4 Limit on mediator mass

For the vector mediator modes as described in subsection 3.1.7 limits on which models can be excluded have been calculated. This is done by calculating which models the p-value is < 0.05. This is done using the two different error models as described in subsection 3.1.5 as figures of merit. All signals which have been used can be found in A.2.3.
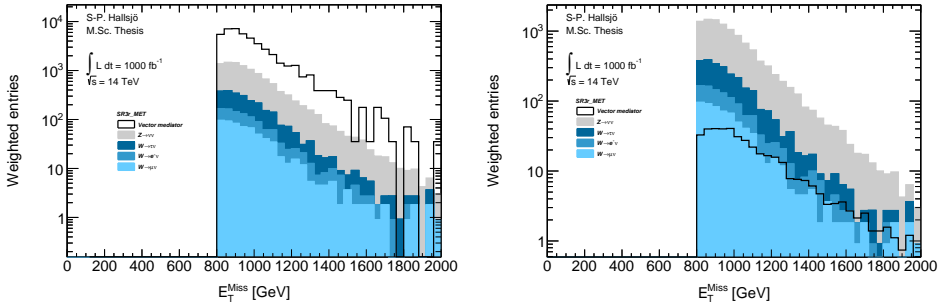


**(a)** *A signal model given in log-scale which is not blocked by the amound of background and is thus excludable.*

**(b)** *A signal model given in log-scale which is blocked by the amound of background and is thus nonexcludable.*

**Figure 3.3:** *Signal on background plot for $E_T^{Miss}$ on reco level in SR3 to illustrate a signal which is excludable and one which is not.*

To set a limit on the mediator mass the p-value is calculated in different signal regions for the different signal models with different mediator mass. As an example a plot of this in signal region d is given in figure 3.4 where the p-value of the models is plotted against the increasing mediator mass for different widths and dark matter masses. The result of which models are excludable, thus with a p-value< 0.05 are given in tables 3.11 and 3.12.
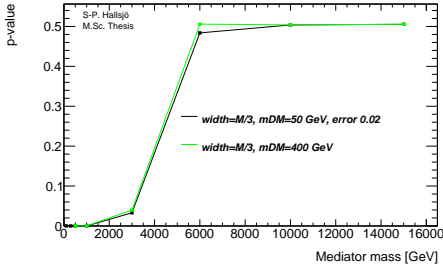
**(a)** *P-values at reco level for different mediator masses and dark matter masses at a width of m/3.*
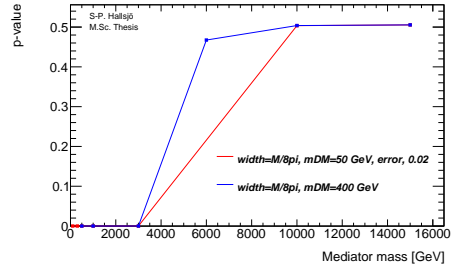
**(b)** *P-values at reco level for different mediator masses and dark matter masses at a width of m/8π.*

**Figure 3.4:** *P-values at reco level for the the different mediator masses, dark matter masses and different widths which were investigated in SRd.*

| width | mDM=50 GeV | mDM=400 GeV |
|-------|------------|-------------|
| m/3   | 1000 GeV   | 1000 GeV    |
| m/8π  | 3000 GeV   | 3000 GeV    |

**Table 3.11:** *Limits on which the highest mediator mass which can be excluded for different widths, different dark matter masses for truth and reco and both error models. In SR2, 3, 4, c, d.*

| width | mDM=50 GeV | mDM=400 GeV |
|-------|------------|-------------|
| m/3   | 1000 GeV   | 1000 GeV    |
| m/8p  | 1000 GeV   | 1000 GeV    |

**Table 3.12:** *Limits on which the highest mediator mass which can be excluded for different widths, different dark matter masses for truth and reco and both error models. In SRb.*

What can be seen in the tables is that the models are very robust when it comes to increased fluctuation in the background as indicated by the error models and with the introduction of pile-up. It is though quite interesting to see that SRb is the signal region which was worst suited for the vector mediator signals. Which by looking at the definition would suggest that the background is less susceptible to a lead jet cut than the signals.

## 3.5  Discussion

### 3.5.1  Comparison to previous results

The background was compared to Ref. [33] altering the cross-sections of the samples used in this thesis to simulate a center of mass energy of 8 TeV instead of 14. This could unfortunately not be done for the signals as that would require new samples to be produced. As seen and some what discussed in subsection 3.4.1 the events corresponded quite nicely to the values from the paper. The discrepancies are explained by general differences between simulations and measured events, such as:

- The difference in W$\to \tau\nu$ can be explained by the fact that $\tau$ can not be recreated as a jet in the simulated events which it can in measured events.

- The difference in W$\to \mu\nu$ is explained through the simulated events having a better separation of muons neutrinos and $E_T^{Miss}$.

Where the choice of a new muon veto giving more events supports the final claim.

In table 3.13 the limits for the mass suppresion scale are given from both the paper and from this work. It is seen that the increase in luminosity and center of mass energy gives an increase of the mass supression scale by a factor of 2-3.

| Dark matter mass | From simulation | From paper |
|---|---|---|
| 50 GeV | 1960 GeV | 800 GeV |
| 400 GeV | 1871 GeV | 700 GeV |

**Table 3.13:** *M\* values in SR2 from both simulation at 14 TeV, 1000fb$^{-1}$ and from Ref. [33] at 8 TeV and 10fb$^{-1}$.*

### 3.5.2  Effect of the high luminosity

As seen in section 3.4, the effect of a pile-up rate of 140 is minute in the signal regions chosen. The primary focus of this thesis was to look at the effect of pile-up, and try to mitigate the effect of it. However it is shown here that by choosing signal regions with a high enough requirement the effect is minute. Thus the focus was shifted to perform a more in-depth mono-jet analysis of different Dm signal models. This models were specifically the vector mediators.

For the mass suppression scale, as seen in subsection 3.4.3, comparing the truth values against the reco values the difference is at most < 5%. Thus these signal regions are preferable for use in the high luminosity upgrade.

Regarding the mediator models, as discussed in subsection 3.4.4 the models are sensitive to exclusion regardless of truth or reco. This suggests that the different models are very robust or that the effect of pile-up is negligible. However the later is more probable since a tougher error model produces the same results.

## 3.6   Conclusion

### 3.6.1   Limit on M*

The limits can be found in subsection 3.4.3 and are 2-3 times better than previous results at 8 TeV and $10\text{fb}^{-1}$.

### 3.6.2   Limit on mediator mass

The limits can be found in subsection 3.4.4 and is the first result done with these models and thus can not be compared.

### 3.6.3   Effect of the high luminosity

At a pile-up level of 140 the effect is at most < 5% for the mass suppression scale and does not affect the vector mediator models which are robust as discussed in subsection 3.5.2.

# 4

## Results and Conclusions

**Disclaimer: This chapter is not yet complete.**

## 4.1 Validation of smearing functions

Have some discussion.

Result they appear to work as expected, the reference paper was a bit unclear, I leave my writing as a better reference.

## 4.2   Signal to background ratio

### 4.2.1   Limit on M*

### 4.2.2   Limit on mediator mass

## 4.3   Other selection criteria and observables

### 4.3.1   Limit on M*

### 4.3.2   Limit on mediator mass

## 4.4   Mitigating the effect of the high luminosity

## 4.5   Recommendations to mitigate the effect of the high luminosity

Keep to a higher energy region, or signal region.

## 4.6   Suggestions for future research

With more time, search for new signal regions, the only solution now for the HL is to go up in energy. Since none of the other parameters (eta,phi etc) seem to be altered these can not be used. Is there something that has been overlooked?

Test the effect of pile-up for lower signal regions? See if the effect is as big as predicted.

Explore other theoretical models for dark matter, other d operators etc. Models that are based on Supersymmetry and not just effective theories.

Create more similar signal regions to be able to compare to the 20fb paper.

Sätt av ett kort kapitel sist i rapporten till att avrunda och föreslå rikningar för framtida utveckling av arbetet.

# Appendix

# A

## Datasets

**Disclaimer: This appendix is not yet complete.**

## A.1 Background processes

All datasets used are d4pd which is a dataformat used at CERN.

### A.1.1 Validation

For the validation the following datasets were used, with a filter at generator level at 450GeV for lead jet and MET.

157539 sherpa ct10 znunupt280 157534 sherpa ct10 wenupt200
157535 sherpa ct10 wmunupt200
157536 sherpa ct10 wtaunupt200
129160 pythia8 au2cteq6l1 perf jf17
129160 pythia8 au2cteq6l1 perf jf17
129170 pythia8 au2cteq6l1 gammajet dp17

They should be read as such: Monte Carlo version, dataset number, generator, ? name.

### A.1.2 Background to signals

The same as the above though now with the filter as indicated by their name. The second znunu sample has been generated with and center of mass energy at 8 TeV.

157539 sherpa ct10 znunupt280
157539 8tev sherpa ct10 znunupt280

944 157536 sherpa ct10 wtaunupt200
945 157534 sherpa ct10 wenupt200
946 157535 sherpa ct10 wmunupt200

947 ## A.2  Signals

948 ### A.2.1  Qcut

949 Qcut means that the original data has been split into different parts depending
950 on the value of the lead jet pt.

951 ### A.2.2  D5 signal processes

952 188408 madgraphpythia auet2bcteq6l1 d5 dm50 ms10000 qcut200
953 188409 madgraphpythia auet2bcteq6l1 d5 dm50 ms10000 qcut400
954 188410 madgraphpythia auet2bcteq6l1 d5 dm50 ms10000 qcut600

955 188411 madgraphpythia auet2bcteq6l1 d5 dm400 ms10000 qcut200
956 188412 madgraphpythia auet2bcteq6l1 d5 dm400 ms10000 qcut400
957 188413 madgraphpythia auet2bcteq6l1 d5 dm400 ms10000 qcut600

958 **All signals should be read as such: Monte Carlo version, dataset number, gen-**
959 **erator, ?, name of operator, dark matter mass, default mass suppression scale,**
960 **qcut part.** As discussed in **reference**

961 ### A.2.3  Light vector mediator processes

962 188414 madgraphpythia auet2bcteq6l1 dmv dm50 mm100 w3 qcut200
963 188422 madgraphpythia auet2bcteq6l1 dmv dm50 mm100 w3 qcut400
964 188430 madgraphpythia auet2bcteq6l1 dmv dm50 mm100 w3 qcut600

965 188415 madgraphpythia auet2bcteq6l1 dmv dm50 mm300 w3 qcut200
966 188423 madgraphpythia auet2bcteq6l1 dmv dm50 mm300 w3 qcut400
967 188431 madgraphpythia auet2bcteq6l1 dmv dm50 mm300 w3 qcut600

968 188416 madgraphpythia auet2bcteq6l1 dmv dm50 mm500 w3 qcut200
969 188424 madgraphpythia auet2bcteq6l1 dmv dm50 mm500 w3 qcut400
970 188432 madgraphpythia auet2bcteq6l1 dmv dm50 mm500 w3 qcut600

971 188417 madgraphpythia auet2bcteq6l1 dmv dm50 mm1000 w3 qcut200
972 188425 madgraphpythia auet2bcteq6l1 dmv dm50 mm1000 w3 qcut400
973 188433 madgraphpythia auet2bcteq6l1 dmv dm50 mm1000 w3 qcut600

974 188418 madgraphpythia auet2bcteq6l1 dmv dm50 mm3000 w3 qcut200
975 188426 madgraphpythia auet2bcteq6l1 dmv dm50 mm3000 w3 qcut400
976 188434 madgraphpythia auet2bcteq6l1 dmv dm50 mm3000 w3 qcut600

977 188419 madgraphpythia auet2bcteq6l1 dmv dm50 mm6000 w3 qcut200
978 188427 madgraphpythia auet2bcteq6l1 dmv dm50 mm6000 w3 qcut400
979 188435 madgraphpythia auet2bcteq6l1 dmv dm50 mm6000 w3 qcut600

980   188420 madgraphpythia auet2bcteq6l1 dmv dm50 mm10000 w3 qcut200
981   188428 madgraphpythia auet2bcteq6l1 dmv dm50 mm10000 w3 qcut400
982   188436 madgraphpythia auet2bcteq6l1 dmv dm50 mm10000 w3 qcut600

983   188421 madgraphpythia auet2bcteq6l1 dmv dm50 mm15000 w3 qcut200
984   188429 madgraphpythia auet2bcteq6l1 dmv dm50 mm15000 w3 qcut400
985   188437 madgraphpythia auet2bcteq6l1 dmv dm50 mm15000 w3 qcut600

986   188438 madgraphpythia auet2bcteq6l1 dmv dm50 mm100 w8pi qcut200
987   188446 madgraphpythia auet2bcteq6l1 dmv dm50 mm100 w8pi qcut400
988   188454 madgraphpythia auet2bcteq6l1 dmv dm50 mm100 w8pi qcut600

989   188439 madgraphpythia auet2bcteq6l1 dmv dm50 mm300 w8pi qcut200
990   188447 madgraphpythia auet2bcteq6l1 dmv dm50 mm300 w8pi qcut400
991   188455 madgraphpythia auet2bcteq6l1 dmv dm50 mm300 w8pi qcut600

992   188440 madgraphpythia auet2bcteq6l1 dmv dm50 mm500 w8pi qcut200
993   188448 madgraphpythia auet2bcteq6l1 dmv dm50 mm500 w8pi qcut400
994   188456 madgraphpythia auet2bcteq6l1 dmv dm50 mm500 w8pi qcut600

995   188441 madgraphpythia auet2bcteq6l1 dmv dm50 mm1000 w8pi qcut200
996   188449 madgraphpythia auet2bcteq6l1 dmv dm50 mm1000 w8pi qcut400
997   188457 madgraphpythia auet2bcteq6l1 dmv dm50 mm1000 w8pi qcut600

998   188442 madgraphpythia auet2bcteq6l1 dmv dm50 mm3000 w8pi qcut200
999   188450 madgraphpythia auet2bcteq6l1 dmv dm50 mm3000 w8pi qcut400
1000  188458 madgraphpythia auet2bcteq6l1 dmv dm50 mm3000 w8pi qcut600

1001  188444 madgraphpythia auet2bcteq6l1 dmv dm50 mm10000 w8pi qcut200
1002  188452 madgraphpythia auet2bcteq6l1 dmv dm50 mm10000 w8pi qcut400
1003  188460 madgraphpythia auet2bcteq6l1 dmv dm50 mm10000 w8pi qcut600

1004  188445 madgraphpythia auet2bcteq6l1 dmv dm50 mm15000 w8pi qcut200
1005  188453 madgraphpythia auet2bcteq6l1 dmv dm50 mm15000 w8pi qcut400
1006  188461 madgraphpythia auet2bcteq6l1 dmv dm50 mm15000 w8pi qcut600

1007  188462 madgraphpythia auet2bcteq6l1 dmv dm400 mm500 w3 qcut200
1008  188468 madgraphpythia auet2bcteq6l1 dmv dm400 mm500 w3 qcut400
1009  188474 madgraphpythia auet2bcteq6l1 dmv dm400 mm500 w3 qcut600

1010  188463 madgraphpythia auet2bcteq6l1 dmv dm400 mm1000 w3 qcut200
1011  188469 madgraphpythia auet2bcteq6l1 dmv dm400 mm1000 w3 qcut400
1012  188475 madgraphpythia auet2bcteq6l1 dmv dm400 mm1000 w3 qcut600

1013  188464 madgraphpythia auet2bcteq6l1 dmv dm400 mm3000 w3 qcut200
1014  188470 madgraphpythia auet2bcteq6l1 dmv dm400 mm3000 w3 qcut400
1015  188476 madgraphpythia auet2bcteq6l1 dmv dm400 mm3000 w3 qcut600

1016  188465 madgraphpythia auet2bcteq6l1 dmv dm400 mm6000 w3 qcut200
1017  188471 madgraphpythia auet2bcteq6l1 dmv dm400 mm6000 w3 qcut400
1018  188477 madgraphpythia auet2bcteq6l1 dmv dm400 mm6000 w3 qcut600

1019  188466 madgraphpythia auet2bcteq6l1 dmv dm400 mm10000 w3 qcut200
1020  188472 madgraphpythia auet2bcteq6l1 dmv dm400 mm10000 w3 qcut400
1021  188478 madgraphpythia auet2bcteq6l1 dmv dm400 mm10000 w3 qcut600

1022  188467 madgraphpythia auet2bcteq6l1 dmv dm400 mm15000 w3 qcut200
1023  188473 madgraphpythia auet2bcteq6l1 dmv dm400 mm15000 w3 qcut400
1024  188479 madgraphpythia auet2bcteq6l1 dmv dm400 mm15000 w3 qcut600

1025  188480 madgraphpythia auet2bcteq6l1 dmv dm400 mm500 w8pi qcut200
1026  188486 madgraphpythia auet2bcteq6l1 dmv dm400 mm500 w8pi qcut400
1027  188492 madgraphpythia auet2bcteq6l1 dmv dm400 mm500 w8pi qcut600

1028  188481 madgraphpythia auet2bcteq6l1 dmv dm400 mm1000 w8pi qcut200
1029  188487 madgraphpythia auet2bcteq6l1 dmv dm400 mm1000 w8pi qcut400
1030  188493 madgraphpythia auet2bcteq6l1 dmv dm400 mm1000 w8pi qcut600

1031  188482 madgraphpythia auet2bcteq6l1 dmv dm400 mm3000 w8pi qcut200
1032  188488 madgraphpythia auet2bcteq6l1 dmv dm400 mm3000 w8pi qcut400
1033  188494 madgraphpythia auet2bcteq6l1 dmv dm400 mm3000 w8pi qcut600

1034  188483 madgraphpythia auet2bcteq6l1 dmv dm400 mm6000 w8pi qcut200
1035  188489 madgraphpythia auet2bcteq6l1 dmv dm400 mm6000 w8pi qcut400
1036  188495 madgraphpythia auet2bcteq6l1 dmv dm400 mm6000 w8pi qcut600

1037  188484 madgraphpythia auet2bcteq6l1 dmv dm400 mm10000 w8pi qcut200
1038  188490 madgraphpythia auet2bcteq6l1 dmv dm400 mm10000 w8pi qcut400
1039  188496 madgraphpythia auet2bcteq6l1 dmv dm400 mm10000 w8pi qcut600

1040  188485 madgraphpythia auet2bcteq6l1 dmv dm400 mm15000 w8pi qcut200
1041  188491 madgraphpythia auet2bcteq6l1 dmv dm400 mm15000 w8pi qcut400
1042  188497 madgraphpythia auet2bcteq6l1 dmv dm400 mm15000 w8pi qcut600

# Bibliography

[1] Collaboration ATLAS. Letter of Intent for the Phase-II Upgrade of the ATLAS Experiment. Dec 2012. URL `https://cds.cern.ch/record/1502664/`. Cited on pages 1, 17, 26, and 28.

[2] B.H. Bransden and C.J. Joachain. *Quantum mechanics*. Pearson Education, second edition, 2000. Cited on page 3.

[3] S-P. Hallsjö. Covering the sphere with noncontextuality inequalities. Bachelor's thesis, Linköping University, The Institute of Technology, 2013. URL `http://urn.kb.se/resolve?urn=urn:nbn:se:liu:diva-103663`. Cited on page 3.

[4] A. Zee. *Quantum Field Theory in a Nutshell*. Princeton University Press, illustrated edition edition, March 2003. ISBN 0691010196. Cited on pages 3, 4, 7, and 8.

[5] H. Goldstein, C. P. Poole, and J. L. Safko. *Classical Mechanics (3rd Edition)*. Addison-Wesley, 3 edition, June 2001. ISBN 0201657023. Cited on page 3.

[6] W. Herr and B. Muratori. Concept of luminosity. 2006. URL `http://cds.cern.ch/record/941318/`. Cited on pages 3 and 4.

[7] W. E. Burcham and M. Jobes. *Nuclear and Particle Physics*. Pearson education, second edition, 1995. Cited on page 4.

[8] The ATLAS Collaboration. Observation of a new particle in the search for the Standard Model Higgs boson with the ATLAS detector at the LHC. *Phys. Lett. B*, 716(arXiv:1207.7214. CERN-PH-EP-2012-218):1–29. 39 p, Aug 2012. Cited on page 4.

[9] Serguei Chatrchyan et al. Observation of a new boson at a mass of 125 GeV with the CMS experiment at the LHC. *Phys.Lett.*, B716:30–61, 2012. doi: 10.1016/j.physletb.2012.08.021. Cited on page 4.

[10] Standard model of elementary particles. `http://en.wikipedia.org/wiki/File:Standard_Model_of_Elementary_Particles.svg`, 2014. Accessed: 2014-03-24. Cited on page 5.

[11] G. Jungman, M. Kamionkowski, and K. Griest. Supersymmetric dark matter. *Physics Reports*, 267:195–373, March 1996. doi: 10.1016/0370-1573(95) 00058-5. Cited on pages 4 and 7.

[12] V. Trimble. Existence and nature of dark matter in the universe. *Annual Review of Astronomy and Astrophysics*, 25(1):425–472, 1987. doi: 10.1146/annurev.aa.25.090187.002233. URL `http://dx.doi.org/10.1146/annurev.aa.25.090187.002233`. Cited on page 5.

[13] F. Zwicky. Die Rotverschiebung von extragalaktischen Nebeln. *Helvetica Physica Acta*, 6:110–127, 1933. Cited on page 6.

[14] NASA. NASA's solar system exploration: the planets: orbits and physical characteristics. `https://solarsystem.nasa.gov/planets/charchart.cfm`, 2014. Accessed: 2014-03-21. Cited on page 6.

[15] T. S. van Albada, J. N. Bahcall, K. Begeman, and R. Sancisi. Distribution of dark matter in the spiral galaxy NGC 3198. *Astrophysical Journal*, 295: 305–313, August 1985. doi: 10.1086/163375. Cited on page 6.

[16] P. Gondolo. Non-baryonic dark matter. *NATO Sci.Ser.II*, 187:279–333, 2005. Cited on page 6.

[17] J. Goodman, M. Ibe, A. Rajaraman, W. Shepherd, Tim M.P. Tait, et al. Constraints on Light Majorana dark Matter from Colliders. *Phys.Lett.*, B695: 185–188, 2011. doi: 10.1016/j.physletb.2010.11.009. Cited on pages 7 and 8.

[18] ATLAS Collaboration. Search for dark matter candidates and large extra dimensions in events with a jet and missing transverse momentum with the atlas detector. *J. High Energy Phys.*, 04(arXiv:1210.4491. CERN-PH-EP-2012-210):075. 58 p, October 2012. URL `http://cds.cern.ch/record/1485031`. Cited on pages 7, 8, and 10.

[19] J. Goodman, M. Ibe, A. Rajaraman, W. Shepherd, T. M. P. Tait, and H.-B. Yu. Constraints on dark matter from colliders. *Phys.Rev.D82:116010,2010*, 82 (11):116010, December 2010. doi: 10.1103/PhysRevD.82.116010. Cited on pages 7 and 8.

[20] ATLAS. Atlas luminosity public results. `https://twiki.cern.ch/twiki/bin/view/AtlasPublic/LuminosityPublicResults`, 2013. Accessed: 2014-03-06. Cited on page 11.

[21] AC Team. The four main LHC experiments, Jun 1999. URL `http://cds.cern.ch/record/40525`. Cited on page 11.

[22] The ATLAS Collaboration. The atlas experiment at the cern large hadron collider. *Journal of Instrumentation*, 3(08):S08003. 437 p, 2008. URL `https://cdsweb.cern.ch/record/1129811/`. Cited on page 12.

[23] J. Pequenao. Computer generated image of the whole ATLAS detector, Mar 2008. URL `http://cds.cern.ch/record/1095924`. Cited on page 13.

[24] ATLAS Collaboration. Event display for one of the monojet candidates in the data. The event has a jet with pt = 602 GeV at eta = -1 and phi = 2.6, MET = 523 GeV, and no additional jet with ptjet > 30 GeV in the final state. `https://atlas.web.cern.ch/Atlas/GROUPS/PHYSICS/CONFNOTES/ATLAS-CONF-2011-096/fig_08.png`, 2011. Accessed: 2014-03-28. Cited on page 14.

[25] ATLAS Collaboration. Physics at a High-Luminosity LHC with ATLAS. Jul 2013. URL `https://cds.cern.ch/record/1564937`. Cited on page 16.

[26] J. Alwall, M. Herquet, F. Maltoni, O. Mattelaer, and T. Stelzer. MadGraph 5: going beyond. *Journal of High Energy Physics*, 6:128, June 2011. doi: 10.1007/JHEP06(2011)128. Cited on pages 16 and 33.

[27] T. Gleisberg, S. Hoeche, F. Krauss, A. Schalicke, S. Schumann, et al. SHERPA 1. alpha: A Proof of concept version. *JHEP*, 0402:056, 2004. doi: 10.1088/1126-6708/2004/02/056. Cited on page 16.

[28] T. Sjöstrand, S. Mrenna, and P. Skands. A brief introduction to {PYTHIA} 8.1. *Computer Physics Communications*, 178(11):852 – 867, 2008. ISSN 0010-4655. doi: http://dx.doi.org/10.1016/j.cpc.2008.01.036. URL `http://www.sciencedirect.com/science/article/pii/S0010465508000441`. Cited on pages 16 and 33.

[29] The ROOT Team. Root. `http://root.cern.ch/drupal/`, 2014. Accessed: 2014-03-28. Cited on page 16.

[30] S. Agostinelli, J. Allison, K. Amako, et al. Geant4—a simulation toolkit. *Nuclear Instruments and Methods in Physics Research Section A: Accelerators, Spectrometers, Detectors and Associated Equipment*, 506(3):250 – 303, 2003. ISSN 0168-9002. doi: http://dx.doi.org/10.1016/S0168-9002(03)01368-8. URL `http://www.sciencedirect.com/science/article/pii/S0168900203013688`. Cited on page 17.

[31] ATLAS Collaboration. Performance assumptions for an upgraded ATLAS detector at a High-Luminosity LHC. Mar 2013. URL `https://cds.cern.ch/record/1527529/`. Cited on pages 17, 20, 26, 27, and 28.

[32] ATLAS Collaboration. Electron performance measurements with the ATLAS detector using the 2010 LHC proton-proton collision data. *Eur. Phys. J. C*, 72(arXiv:1110.3174. CERN-PH-EP-2011-117):1909. 45 p, Oct 2011. Comments: 33 pages plus author list (45 pages total), 24 figures, 12 tables, submitted to Eur. Phys. J. C. Cited on pages 26 and 28.

[33] ATLAS Collaboration. Search for New Phenomena in Monojet plus Missing Transverse Momentum Final States using 10fb-1 of pp Collisions at sqrts=8 TeV with the ATLAS detector at the LHC. Nov 2012. URL `http://cds.cern.ch/record/1493486/`. Cited on pages 32, 33, 34, 36, 37, and 43.